Author/s:
Skopkova, M;Hennig, F;Shin, BS;Turner, CE;Stanikova, D;Brennerova, K;Stanik, J;Fischer, U;Henden, L;Müller, U;Steinberger, D;Leshinsky-Silver, E;Bottani, A;Kurdiova, T;Ukropec, J;Nyitrayova, O;Kolnikova, M;Klimes, I;Borck, G;Bahlo, M;Haas, SA;Kim, JR;Lotspeich-Cole, LE;Gasperikova, D;Dever, TE;Kalscheuer, VM

Title:
EIF2S3 Mutations Associated with Severe X-Linked Intellectual Disability Syndrome MEHMO

Date:
2017-04-01

Citation:
Skopkova, M., Hennig, F., Shin, B. S., Turner, C. E., Stanikova, D., Brennerova, K., Stanik, J., Fischer, U., Henden, L., Müller, U., Steinberger, D., Leshinsky-Silver, E., Bottani, A., Kurdiova, T., Ukropec, J., Nyitrayova, O., Kolnikova, M., Klimes, I., Borck, G. ,... Kalscheuer, V. M. (2017). EIF2S3 Mutations Associated with Severe X-Linked Intellectual Disability Syndrome MEHMO. Human Mutation, 38 (4), pp.409-425. https://doi.org/10.1002/humu.23170.

EIF2S3 mutations associated with severe X-linked intellectual disability syndrome MEHMO

Martina Skopkova[1]*, Friederike Hennig[2]*, Byung-Sik Shin[3*], Clesson E. Turner[4], Daniela Stanikova[1,5], Katarina Brennerova[5], Juraj Stanik[1,5,6], Ute Fischer[2], Lyndal Henden[7,8], Ulrich Müller[9], Daniela Steinberger[9,10], Esther Leshinsky-Silver[11,12,13], Armand Bottani[14], Timea Kurdiova[1], Jozef Ukropec[1], Olga Nyitrayova[15], Miriam Kolnikova[16], Iwar Klimes[1], Guntram Borck[17], Melanie Bahlo[7,8], Stefan A. Haas[18], Joo-Ran Kim[3], Leda E. Lotspeich-Cole[3], Daniela Gasperikova[1**#], Thomas E. Dever[3**#], Vera M. Kalscheuer[2**#]

* These authors contributed equally
**These authors supervised equally
To whom correspondence should be addressed

[1]DIABGENE & Laboratory of Diabetes and Metabolic Disorders, Institute of Experimental Endocrinology, Biomedical Research Center, Slovak Academy of Sciences, Bratislava, Slovakia
[2]Research Group Development and Disease, Max Planck Institute for Molecular Genetics, Berlin, Germany
[3]*Eunice Kennedy Shriver* National Institute of Child Health and Human Development, National Institutes of Health, Bethesda, Maryland 20892, USA
[4]Department of Genetics, Walter Reed National Military Medical Center, Bethesda, Maryland 20889, USA
[5]First Department of Pediatrics, Medical Faculty of Comenius University, Bratislava, Slovakia
[6]Center for Pediatric Research Leipzig, Hospital for Children & Adolescents, University of Leipzig, Germany
[7]Population Health and Immunity Division, The Walter and Eliza Hall Institute of Medical Research, Melbourne, VIC, Australia
[8]Department of Medical Biology, University of Melbourne, Melbourne, VIC, Australia
[9]Institut für Humangenetik, Justus-Liebig-Universität Giessen, 35392 Giessen, Germany
[10]bio.logis Center for Human Genetics, 60438 Frankfurt a. M., Germany
[11]Institute of Medical Genetics, Wolfson Medical Center, Holon, Israel
[12]Metabolic-Neurogenetic Clinic, Wolfson Medical Center, Holon, Israel
[13]Molecular Genetics Laboratory, Wolfson Medical Center, Holon, Israel
[14]Service of Genetic Medicine, Geneva University Hospitals, Geneva, Switzerland
[15]Cytophatos, Bratislava, Slovakia
[16]Department of Pediatric Neurology, Medical Faculty of Comenius University, Bratislava, Slovakia
[17]Institute of Human Genetics, University of Ulm, Ulm, Germany

[18]Department of Computational Molecular Biology, Max Planck Institute for Molecular Genetics, Berlin, Germany

Grant numbers:

2/0166/14, APVV-187-12, 26240220051, 241995, APP1102971 and APP1054618

Corresponding Authors:

Daniela Gasperikova, DIABGENE & Laboratory of Diabetes and Metabolic Disorders, Institute of Experimental Endocrinology, Biomedical Research Center, Slovak Academy of Sciences, Dubravska cesta 9, 84505, Bratislava, Slovakia. Phone: +421 905 681 978, Email: daniela.gasperikova@savba.sk

Thomas E. Dever, NICHD, National Institutes of Health, 6 Center Dr, Bldg. 6, Rm 228, Bethesda, MD 20892 USA. Tel. 301-496-4519; Email: thomas.dever@nih.gov

Vera M. Kalscheuer, Max Planck Institute for Molecular Genetics, Research Group Development and Disease, Ihnestr. 73, D-14195 Berlin, Germany. Telephone: (49) 30 8413 1293; FAX: (49) 30 8413 1383; Email: kalscheu@molgen.mpg.de

Running title: *EIF2S3* mutations cause MEHMO syndrome

Abstract

Impairment of translation initiation and its regulation within the integrated stress response (ISR) and related unfolded-protein response has been identified as a cause of several multi-systemic syndromes. Here we link MEHMO syndrome, whose genetic etiology was unknown, to this group of disorders. MEHMO is a rare X-linked syndrome characterized by profound intellectual disability, epilepsy, hypogonadism, and hypogenitalism, microcephaly, and obesity. We have identified a C-terminal frameshift mutation (Ile465Serfs) in the *EIF2S3* gene in three families with MEHMO syndrome and a novel maternally inherited missense *EIF2S3* variant (c.324T>A; p.Ser108Arg) in another male patient with less severe clinical symptoms. The

EIF2S3 gene encodes the γ subunit of eukaryotic translation initiation factor 2 (eIF2), crucial for initiation of protein synthesis and regulation of the ISR. Studies in patient fibroblasts confirm increased ISR activation due to the Ile465Serfs mutation and functional assays in yeast demonstrate that the Ile465Serfs mutation impairs eIF2γ function to a greater extent than tested missense mutations, consistent with the more severe clinical phenotype of the Ile465Serfs male mutation carriers. Thus, we propose that more severe *EIF2S3* mutations cause the full MEHMO phenotype, while less deleterious mutations cause a milder form of the syndrome with only a subset of the symptoms.

Key words: MEHMO syndrome, XLID, *EIF2S3*, translation initiation, integrated stress response, unfolded-protein response

Introduction

Neurodevelopmental disorders comprise MEHMO syndrome (MIM# 300148), a rare form of severe X-linked intellectual disability (XLID) with additional clinical symptoms including microcephaly, epileptic seizures, hypogonadism, hypogenitalism, diabetes and obesity. The acronym MEHMO was coined by Steinmüller et al. (Steinmuller, et al., 1998) who described a large three-generation family with five affected boys and assigned the disease locus to the short arm of chromosome X (Xp11.3-22.13). Only three other affected individuals from two families were clinically described and communicated in the literature (DeLozier-Blanchet, et al., 1999; Delozier-Blanchet, et

al., 1989; Leshinsky-Silver, et al., 2002). Till now, the genetic cause of this condition has not been resolved.

We took advantage of next generation sequencing in three unreported families with this condition, in addition to the family reported by Steinmüller et al (Steinmuller, et al., 1998), to identify the underlying genetic cause of this severe disorder. We report that in these families MEHMO syndrome is associated with frameshift and missense mutations in the X chromosome gene *EIF2S3*. We previously identified a missense mutation in *EIF2S3* present in a consanguineous family with XLID (MIM# 300987) (Borck, et al., 2012), and while this manuscript was in preparation, two novel *EIF2S3* mutations were reported in two unrelated families with variable XLID (MIM# 300987) (Moortgat, et al., 2016).

EIF2S3 encodes the γ subunit of the heterotrimeric eukaryotic translation initiation factor eIF2, which forms a stable ternary complex (TC) with GTP and the initiator methionyl-tRNA (Met-$tRNA_i^{Met}$). The eIF2–GTP–Met-$tRNA_i^{Met}$ TC binds along with the factors eIF1, eIF1A, eIF3 and eIF5 to the small 40S ribosomal subunit to form a 43S preinitiation complex (PIC). Subsequent binding of this complex to an mRNA forms a 48S PIC. According to the scanning model of translation initiation, the 43S PIC first associates with the 5' end of an mRNA and then linearly scans in a 3' direction to select a translation start site (Hinnebusch, 2011). Base-pairing interactions between the anticodon loop of $tRNA_i^{Met}$ and an AUG codon of the mRNA triggers the ribosome to stop scanning, promotes completion of GTP hydrolysis by eIF2, and prompts release of eIF2–GDP from the complex. Conformational changes in the ribosome accompanying these events culminate in joining of the large 60S ribosomal subunit to form the 80S initiation complex that is poised to begin

translation elongation, the codon-dependent stepwise addition of amino acids to the growing polypeptide chain (Hinnebusch, 2014).

The active eIF2–GTP is regenerated by the guanine nucleotide exchange factor eIF2B. This is a key control point for eukaryotic protein synthesis. Phosphorylation of the α subunit of eIF2 by members of a family of stress-responsive protein kinases impairs general translation yet enhances the translation of specific mRNAs in a process known as general amino acid control in yeast (Dever, 2002; Hinnebusch, 2005) or as the integrated stress response (ISR) in other organisms (Dever, 2002; Dever, 2007; Harding, et al., 2000; Harding, et al., 2003; Pavitt, et al., 2012). The eIF2α kinase PERK feeds into the ISR by sensing endoplasmic reticulum (ER) stress and triggering the translational arm of the unfolded-protein response (UPR), to alleviate the burden of misfolded protein accumulation. The phosphorylation of eIF2α converts eIF2 into an inhibitor of eIF2B and thereby limits the availability of eIF2–GTP for TC formation (Hinnebusch, 2005). The decreased TC level impairs global translation, providing the cell time to cope with the stressor, and paradoxically increases the translation of selected mRNAs bearing regulatory upstream open reading frames (uORFs). This class of translationally up-regulated mRNAs includes those encoding the yeast transcription factor *GCN4* and the mammalian activating transcription factor-4 (*ATF4*), which in turn promote expression of genes necessary for the adaptive response to the stress situation (Harding, et al., 2003; Hinnebusch, 2005; Ron, et al., 2007). One of the ATF4 target genes is *DDIT3* encoding the transcription factor C/EBP-homologous protein (CHOP) that plays an essential role in response to a variety of cell stresses by inducing cell cycle arrest or, in the case of unresolved or prolonged stress, apoptosis (Su, et al., 2008; Tabas, et al., 2011). The

ISR and translation control of the *GCN4* and *ATF4* mRNAs have proven to be useful in vivo reporters of eIF2 function (Alone, et al., 2008; Borck, et al., 2012; Harding, et al., 2000; Harding, et al., 2003; Hinnebusch, 2005; Lu, et al., 2004; Vattem, et al., 2004; Young, et al., 2016).

Here, we connect *EIF2S3* with MEHMO syndrome, show via functional assays in yeast and human cells that the *eif2s3/EIF2S3* mutations identified in this study have a deleterious effect on eIF2γ function, and suggest genotype-phenotype relations in affected subjects.

Materials and Methods

Patients

All subjects provided written informed consent for this research study, which was approved by the ethics committees of the participating centers and adhered to the tenets set forth in the Declaration of Helsinki. For subjects under the age of 18 years, written consent was obtained from a parent.

Cell Culture

HEK293-T, HeLa and fibroblast cells were cultured in Dulbecco´s modified Eagle´s medium with 10 % fetal bovine serum, 1 % penicillin/streptomycin and 2 mM glutamine at 37 °C with 5 % CO_2. Transient DNA transfections were carried out using PeqFECT DNA or jetPRIME (both PEQLAB, Erlangen, Germany) according to the manufacturer's instructions.

Next Generation Sequencing and Sanger Sequencing

Genomic DNA of patients and their family members was extracted from peripheral blood using standard procedures. Probands from all families had next generation sequencing performed (whole exome or X chromosome exome). In case of Slovak patients, whole exome sequencing (WES) including basic bioinformatics up to annotated vcf files was performed by service providers. DNA of the index patient from family 1 was sequenced by Theragen BiO Institute (South Korea) on HiSeq2500 (Illumina, San Diego, CA, USA) using SureSelect Whole Human All Exon V4+UTR (Agilent, Santa Clara, CA, USA) for exome capture. Sequencing reads were mapped to hg19 reference using BWA-MEM algorithm and variants were called using GATK UnifiedGenotyper pipeline. Variants with PHRED score quality >10 were annotated using snpEFF and snpSIFT tools. Variants were prioritized according to their population frequency, predicted effect and position on the X chromosome. DNA of the index patient from family 2 and his parents were sequenced by BGI (Hong Kong) using the Human 59M Exon kit and Complete Genomics platform. Base calling, alignment to reference b37, and variant calling was performed using Complete Genomics' specific bioinformatic pipeline by the service provider. The index patient from family 3 had X-chromosome exome sequencing performed as previously described (Hu, et al., 2016). Afterwards, sequencing reads were mapped to hg18 via RazerS as described in Hu et al. (Hu, et al., 2016). Accordingly, short insertions/deletions were called from those primary alignments as well as by applying a split-read mapping approach (SplazerS, (Emde, et al., 2012)). Final variant calls were lifted over to hg19 in order to allow evaluation and prioritization based on more recent gene annotations. WES was performed on DNA of the index

patient from family 4 and his parents by GeneDx (Gaithersburg, Maryland, USA) on HiSeq2500 (Illumina, San Diego, CA, USA) using SureSelect V4+UTR (Agilent Technologies Inc., Santa Clara, CA, USA) for exome capture and on DNA of the patient from family published by DeLozier-Blanchet et al. (DeLozier-Blanchet, et al., 1999; Delozier-Blanchet, et al., 1989) as previously described (Borck, et al., 2012). Conventional Sanger sequencing for mutation search in *EIF2S3* coding exons and flanking intronic sequences, confirmation of variants, segregation studies and haplotyping was performed on ABI 3500 sequencer (Applied Biosystems, Foster City, CA, USA) using standard procedures. Primers can be obtained upon request. For *EIF2S3* cDNA numbering, the A of the ATG translation initiation codon in the GenBank reference sequence NM_001415.3, with the initiation codon as codon 1 was used. For haplotyping of family 1, regions containing positions of 18 previously unreported variants found on chromosome X of the index patient (Supp. Table S1A), as well as 16 SNPs from 11 other regions (Supp. Table S1B), were sequenced in all available members of his family. Haplotypes within the pedigree were resolved manually.

EIF2S3 variants identified through this study were submitted to the LOVD (databases.lovd.nl/shared/genes/EIF2S3; variants EIF2S3_000008 and EIF2S3_000018) and ClinVar (SCV000321299 and SCV000321546) databases.

Identity by Descent (IBD) Analysis

For IBD analysis genotyping was performed using the Illumina Human Omni 2.5 BeadChip (Illumina, San Diego, CA, USA). SNP array data for the index patients from family 1 and 3 and exome data for the index patients from families 1 and 2 and

the mother from family 2 were run through LINKDATAGEN (Bahlo, et al., 2009) with parameter bin=0.0002 to produce a collection of markers with high heterozygosity. XIBD (Henden, et al., 2016) was used to estimate the number of meiosis separating the pair of individuals, the probabilities of sharing zero or one allele IBD, and genomic regions IBD via posterior probabilities and the Viterbi algorithm. SNPs in near perfect linkage disequilibrium ($R^2 \geq 0.99$) and SNPs with minor allele frequencies ≤3 % according to HapMap phase II were removed.

In Silico Analysis

The Clustal Omega alignment was performed using the Uniprot web service (http://www.uniprot.org/align (McWilliam, et al., 2013)). Protein structure analyses were performed using PyMol software (The PyMOL Molecular Graphics System, Version 1.7.6.6 Schrödinger, LLC.). Combined Annotation Dependent Depletion (CADD) tool was used for estimation of variant deleteriousness (Kircher, et al., 2014).

Plasmids for Work in Yeast

The single copy-number *URA3 GCN4-lacZ* plasmid p180 (Hinnebusch, 1985) as well as the single copy-number *URA3 HIS4(AUG)-lacZ* (p367) and *HIS4(UUG)-lacZ* (p391) plasmids (Cigan, et al., 1988) were described previously. The single copy-number *LEU2* plasmid pC2860 that expresses His_8-tagged *GCD11* (yeast eIF2γ) under control of the native promoter (Alone, et al., 2008) as well as the derivatives of pC2860 expressing the mutants *His_8-GCD11-V281K* (pC4187) and His_8-*GCD11-V281T* (pC4188) were described previously (Borck, et al., 2012). Derivatives of pC2860 were generated by site-directed mutagenesis to express *His_8-GCD11-*

D167R (pC5343) as well as the yeast/human eIF2γ chimera *His_8-GCD11(Sc^{1-514}/$Hs^{457-472}$)* (pC5051) and its mutant derivative *His_8-GCD11(Sc^{1-514}/$Hs^{457-472}$)-I465Sfs*4* (pC5052).

Yeast Strains and Genetic Methods

Yeast strains expressing eIF2γ mutants were generated by plasmid shuffling (Boeke, et al., 1987). Briefly, the single copy-number *LEU2* plasmid pC2860 expressing wild-type yeast eIF2γ (*GCD11*) or its mutant derivatives were introduced by transformation into the strain J292 (*MATα leu2-3 leu2-112 ura3-52 his3 gcn2Δ*::*loxP gcd11Δ*::*KanMX* p[*GCD11, URA3*]) (Alone, et al., 2008). The resulting transformants were plated on medium containing 5-fluoroorotic acid (5-FOA) to evict the *URA3* plasmid containing wild type *GCD11* and to leave only the *LEU2* plasmid expressing eIF2γ. For growth assays, the resulting strains were colony purified, grown to saturation in liquid synthetic dextrose (SD) medium containing uracil and histidine, and 4 µl of serial dilutions (of OD_{600} = 1.0, 0.1, 0.01, 0.001, 0.0001) were spotted on SD medium containing the same supplements. Plates were incubated at 30 or 37 °C for 3 days.

For measurement of *GCN4-lacZ* expression, derivatives of strain J292 expressing wild-type or mutant forms of eIF2γ were transformed with the *GCN4-lacZ* plasmid p180. Transformants were grown in SD medium with amino acid supplements to A_{600} ~0.8; and β-galactosidase activities were determined as described previously (Hinnebusch, 1985). To measure the UUG/AUG ratio, the J292 derivatives were transformed with the plasmids p3989 (*HIS4(AUG)-lacZ*) or p3990 (*HIS4(UUG)-lacZ*).

Transformants were grown to A_{600} ~0.8 and β-galactosidase activities were determined. All assays were performed in triplicate at least three times.

RNA Extraction and Reverse Transcription

Total RNA was extracted from $5x10^6$ fibroblast cells using the RNeasy® Plus Mini Kit (Qiagen, Hilden, Germany) according to the manufacturer´s instructions. For qRT-PCR RNA samples were treated with DNaseI (Qiagen, Hilden, Germany) prior to cDNA synthesis. RNA samples were qualitatively assessed and quantified using an Agilent 2100 Bioanalyser with RNA 6000 Nano kit (Agilent Technologies Inc., Santa Clara, CA, USA). cDNA was prepared from 1 µg of total RNA with High-Capacity Reverse Transcription Kit (Applied Biosystems, Foster City, CA, USA) using the random priming method. The mRNA level of *DDIT3* was assessed by RT-qPCR using TaqMan® assays (Hs00358796_g1) and TaqMan® Gene Expression Master Mix on 7900HT Fast Real-Time PCR System (Applied Biosystems, Foster City, CA, USA). Expression was normalized to *YWHAZ* (TaqMan® assay Hs03044281_g1) as a reference gene. Results are presented as 2^{-dCq}. The data were assessed with a two sample t-test (*** $P < 0.001$).

Protein Extraction from Fibroblast Cells

$2x10^6$ patient-derived or control fibroblasts were seeded in 10 cm dishes. After 24 h, cells were washed twice with PBS and incubated with 1 ml lysis buffer containing 50 mM Tris pH 7.5, 100 mM NaCl, 0.1 % NP40 supplemented with EDTA-free protease inhibitors and phosphatase inhibitors (both Roche, Basel, Switzerland) for 15 min on ice. Lysates were then collected and immediately frozen in liquid nitrogen. After thawing the lysates on ice, they were centrifuged at 15000 rcf at 4 °C for 15 min and

the supernatants were concentrated using vivaspin 500 columns (GE Healthcare Life Sciences, Freiburg, Germany) to 100 µl according to the manufacturer´s recommendations.

Plasmids Used for Studies in Mammalian Cells

pCDNA4_EIF2S3 and pCDNA4_EIF2S3_I222T were previously described (Borck et al.). For cloning the EIF2S3 del TCAA construct we used the pCDNA4/TO/myc-HisA vector double digested with EcoRI and XhoI (New England Biolabs) and PCR products generated using pCDNA4_EIF2S3 as template with the following primer pairs: EIF2S3for_EcoRI 5´-TAGAATTCATGGCGGGCGGAGAAGCTGG-3´ and EIF2S3rev_XhoI_CAAT_myc 5´-ATCTCGAGCTGTTGGCTTGTCACTCCTCTTCTTATCTGACCCCAACCAA-3´. For cloning N-terminal FLAG tagged EIF2S3 wild-type and mutant constructs we used the pCMV-Tag 2b vector (STRATAGENE, La Jolla, Ca, USA) double-digested with *Eco*RI and *Xho*I (New England Biolabs, Ipswich, MA, USA) and PCR products generated using pCDNA4_EIF2S3 or pCDNA4_ EIF2S3_delTCAA as template with the following primer pairs: EIF2S3for_EcoRI_FLAG 5´-TAGAATTCGCGGGCGGAGAAGCTGGAG-3´, EIF2S3rev_XhoI_FLAG 5´-ATCTCGAGCTAGTCATCATCTACTGTTG-3´, EIF2S3rev_XhoI_TAAC_FLAG 5´-ATCTCGAGCTACTGTTGGCTTGTCACTC-3´. For cloning N-terminal GFP tagged EIF2S3 wild-type and mutant constructs we used the pEGFP-C2 vector (BD Biosciences Clontech) double-digested with *Eco*RI and *Sal*I (New England Biolabs, Ipswich, MA, USA) and PCR products generated using pCDNA4_EIF2S3 or pCDNA4_ EIF2S3_ΔTAAC as template with the following primer pairs: EIF2S3forw_EcoRI 5´-TAGAATTCATGGCGGGCGGAGAAGCTGG-3´ and

EIF2S3rev_SalI 5`-ATGTCGACCTAGTCATCATCTA-3´ or EIF2S3rev_SalI_TAAC 5´-ATGTCGACCTACTGTTGGCTTG-3´. The p.Ser108Arg derivative was generated by site-directed mutagenesis using the QuikChange II site-directed Mutagenesis Kit (Agilent Technologies Inc., Santa Clara, CA, USA). All constructs were verified by Sanger sequencing.

Transient Expression and Western Blotting

For transient expression experiments, HeLa and HEK293T cells were transfected with 8-12 µg plasmid DNA as described above. 24 h after transfection, cells were collected and resuspended in lysis buffer containing 50 mM Tris pH 8, 150 mM NaCl, 1 % Triton-X100 supplemented with EDTA-free protease inhibitors (Roche, Basel, Switzerland). Supernatants were separated by SDS–PAGE, transferred onto PVDF membranes, blocked with 5 % non-fat milk in PBST and incubated with primary antibody overnight at 4 °C. Membranes were then washed three times with PBST and incubated with HRP-conjugated secondary antibody for 30 min at room temperature followed by chemiluminescence detection.

The following antibodies were used: monoclonal anti-Flag-HRP (A8592, 1:3000, Sigma-Aldrich, St. Louis, MO, USA), polyclonal rabbit anti-EIF2S3 (PA5-31177; 1:1000, Thermo Fischer Scientific, Rockford, IL, USA), monoclonal mouse anti-CHOP (MA1-250; 1:1000, Thermo Fischer Scientific, Rockford, IL, USA), monoclonal mouse anti-Myc antibody (631206, 1:500, Clontech Laboratories, Inc., Mountain View, CA, USA), monoclonal rat anti-tubulin (ab6160 1:20000, Abcam, Cambridge, UK), anti-mouse-HRP (115-035-003, 1:5000, Dianova, Hamburg, Germany) and anti-rabbit-HRP (NA9340, 1:3000 Amersham, Piscataway, NJ, USA). Western blot quantification was performed using ImageJ software.

Immunofluorescence and Confocal Microscopy

HEK293T cells were seeded on laminin/poly-D lysine covered glass cover slips in 6-well plates and were transiently transfected with 2 µg plasmid DNA per well. 24 h after transfection, cells were fixed with 4 % paraformaldehyde, permeated with 0.2 % Triton-X100 and blocked with 3 % bovine serum albumin (BSA) for 1h at room temperature. Incubation with primary monoclonal mouse anti-myc antibody (631206, 1:500, Clontech Laboratories, Inc., Mountain View, CA, USA) was performed at 4 °C overnight followed by detection with the secondary Alexa 594 anti-mouse antibody (A21200, 1:1000, Thermo Fischer Scientific, Rockford, IL, USA) for 1 h at room temperature. Nuclei were counterstained with 0.5 µg/ml DAPI and coverslips were mounted with Fluromount-G (SouthernBiotech, Birmigham, AL, USA). Images were acquired using a Zeiss LSM 700 confocal microscope (Zeiss, Jena, Germany).

Mitochondrial OXPHOS Activities

Activities of complex II and complex IV were measured in saponin permeabilized muscle fibers using oxygen consumption measurements with Clark's electrode (Oxytherm, Hansatech, UK). Approximately 10 mg of muscle was taken into an ice cold relaxing and biopsy preservation solution (BIOPS) prepared as previously described (Larsen, et al., 2014). Briefly, myofibers were gently separated by forceps in ice cold BIOPS and saponin (50 µg/ml) was added for 30 min. Permeabilized sample was transferred into an ice cold mitochondrial respiration medium (MiRO5) prepared as described in (Pesta, et al., 2012). COX activity was assessed as a difference in respiration rate between the complex IV activation state (subsequent addition of 5 mM ascorbate and 0.25 mM TMPD) and the KCN-inactivated state

(3x10 mM KCN). All measurements were made in triplicates. Outer mitochondrial membrane integrity was routinely tested by addition of cytochrome c (19 μM) in the complex IV activated state. Activity of complex II was measured after complex I blocking with rotenone (10 μM) by addition of complex II substrate succinate (10 mM) and ADP (5 mM) and stopped by addition of malonate (1 mM), a complex II inhibitor. Complex II activity was calculated as a difference in respiration rate between the complex II active state and the malonate inactivated state. Three and two patient 1 tissue biological replicates were used for complex II and IV measurements, respectively. Three and nine tissues from control individuals were used for complex II and IV measurements, respectively.

Results

Clinical Phenotypes

Four families with MEHMO syndrome were investigated by massively parallel sequencing to identify the underlying genetic cause. The pedigrees of the families are shown in Figure 1A. Clinical characteristics of all affected males from these families are summarized in Table 1, together with all previously published patients with MEHMO syndrome.

Family 1

The index patient from family 1 was born to non-consanguineous parents of Slovak origin and has one healthy older sister. His mother has sideroblastic anaemia and his maternal grandmother suffered from a heart attack at 54 years, but were otherwise normal. The maternal grandmother had one miscarriage and her brother died in the first months of life of unknown cause. There are no other living male members in the maternal lineage. The proband had prenatally diagnosed

microcephaly at 28th week of gestation. He was delivered at 39+6 gestational weeks with birth length of 47 cm (-2.0 SD) and weight 2920 g (-1.4 SD), Apgar score 8/10 at 5 and 10 minutes and occipitofrontal circumference (OFC) 32 cm (-2.6 SD). Micropenis, cryptorchidism, and peripheral hypertonia were noticed.

Diagnosis of MEHMO was made at the age of 10 months based on the microcephaly, partial complex epileptic seizures (diagnosed at the age of 4 months) resistant to anticonvulsives, hypogenitalism, severe mental and motor delay (corresponding to 3rd month of life), central obesity (rapid weight gain developed after feeding via nasogastric tube inserted due to the dysphagia and hypotrophy at the age of 3 months - BMI SDS increased from -2.1 to +1.0 SD at the age of 8 months, and to +3.7 SD at the age of 2 years), and typical dysmorphic features (full cheeks, large ears, downturned corners of mouth, epiblepharon, long eyelashes and thick eyebrows, tapered fingers and talipes (Figure 1B)).

Other findings. Brain MRI at the age of 4 months showed mild myelination delay corresponding to 2nd-3rd month, and the myelination delay was more pronounced at the age of 19 months with further acute demyelinating changes and cerebral atrophy (Figure 1C). Non-autoimmune diabetes melitus was diagnosed at 10 months and insulin treatment was started. During the first 18 months of life he suffered from repeated episodes (6-8 per year) of acute bronchitis and bronchopneumonia, during which he was lethargic, had worsened diabetes control, and his seizures exacerbated (up to seventy 2-minutes episodes a day before the anti-epileptic treatment was optimized). The seizures were induced also by increased ambient temperature. At age of 17 months, histological examination of muscle biopsy revealed abnormal striated muscle and muscle mitochondria (Figure 1D). Measurements of activities of respiratory chain complexes II and IV in patient 1

muscle (Table 2) showed decreased complex II and normal complex IV activities. For accessory signs see Table 1.

Current status. Currently, at 5 years, his height is 88 cm (-5 SD), weight 15.3 kg (BMI 19.8 kg/m^2, 2.3 SD), head circumference 39 cm (-8.4 SD). Epileptic seizures are well controlled under combination of vigabatrin, phenobarbital, and topimarate treatment. Seizures emerge only during respiratory and urinary infections, which are now less frequent (the patient is under immunoglobulin therapy). He is fed *per os* with additional nasogastric feeding. He has central hypotonia and peripheral hypertonia, and reacts only to strong tactile stimuli.

Family 2

The index patient from family 2 is a 1st child from a Slovak non-consanguineous family with no other affected individuals known. His mother is unaffected. He was delivered in 40+0 gestational weeks with birth length of 49 cm (-0.95 SD) and weight 2440 g (-2.65 SD), Apgar score 8/10 and OFC 29 cm (-5.1 SD).

MEHMO features included microcephaly, therapy resistant seizures (diagnosed at the age of 6 months) without EEG correlation, hypogenitalism, severe mental and motor delay (corresponding to 3rd month of life at the age of 2 years), central obesity, and dysmorphic features very similar to the proband of family 1. He has non-autoimmune diabetes melitus treated with insulin from 10 months. Brain MRI showed myelinization delay at 10 months of age (Figure 1C). For accessory signs see Table 1.

Current status. At the age of 3 years his height is 78 cm (-4.7 SD) and BMI 19.1 kg/m^2 (+1.9 SD). He is hypotonic, with no voluntary movements and he does not show any social interaction.

Family 3

This family has been previously described by Steinmüller et al. (Steinmuller, et al., 1998). The index patient (IV:3) was diagnosed prenatally with microcephaly and was delivered by Caesarean section during the 32nd gestational week with birth weight 1420 g (-0.8 SD), length 40.5 cm (-0,4 SD), OFC 26.5 cm (-1.7 SD). All females from this family who carry the *EIF2S3* mutation on one of their X chromosomes were unaffected.

MEHMO features included microcephaly, therapy resistant epileptic seizures (diagnosed at the age of 7 weeks), hypogenitalism, severe mental and motor delay, central obesity, and dysmorphic features including narrow forehead, full cheeks, facial telangiectasias, downturned corners of the mouth, large ears, edematous hands and feet, tapered fingers, and bilateral talipes. Diabetes was diagnosed at age of 6 months due to a ketoacidotic crisis. For accessory signs see Table 1.

Current status. At 2 years, his height was 74 cm (-4 SD), BMI 19.2 kg/m^2 (+2 SD) and head circumference 37.7 cm (-8.2 SD). Towards the end of his life at 2 years, he had permanent seizures refractory to treatment.

Family 4

The proband is 2nd child from 5th pregnancy (three miscarriages early on in the pregnancies) of non-consanguineous Caucasian parents of Northern European origin living in US with no other affected individuals known including his mother, older brother and younger sister.

MEHMO features included microcephaly, hypospadia and cryptorchidism, developmental delay, and obesity with BMI at the 97th centile (after a longer period of failure to thrive). He does not have epileptic seizures and his EEG was normal.

Current status. At 4 years and 7 months, his height was 93 cm (-3.2 SD), weight 12.3kg (-2.2 SD), BMI 14.2 kg/m^2 (-0.8 SD), and his head circumference was 46.5 cm (-3.4 SD). He has central hypotonia and peripheral hypertonia and spasticity, chronic lung disease, dysphagia, delayed gastric emptying, and grade 5 vesico-ureteral reflux (Table 1).

Exome Sequencing Identified Likely Deleterious Mutations in *EIF2S3*

Index cases from all families (families 1-4) were investigated by massively parallel sequencing. For three patients (families 1, 2 and 4) we performed whole exome sequencing (WES) and included the parents from families 2 and 4. The index patient from family 3 was investigated as part of a larger study on X-chromosome exome resequencing on families with XLID as previously described (Hu, et al., 2016). Sequence analysis indicated that all patients carried a hemizygous mutation in *EIF2S3* located on chromosome X as the most likely disease-relevant change. *EIF2S3* lies in the linkage interval determined for family 3 (Steinmuller, et al., 1998). Strikingly, families 1, 2 and 3 carried the identical 4 bp deletion c.1394_1397delTCAA, which co-segregated with the disease in the families and is predicted to cause a frameshift and a premature stop codon (p.Ile465Serfs*4) in the *EIF2S3* encoded protein eIF2γ. The deletion alters the C-terminus with the last eight amino acids being replaced by three different amino acids (Figure 1E). The patient from family 4 carried a point mutation, c.324T>A, which he inherited from his healthy

mother (Figure 1A) and could not be tested in his healthy brother. The single nucleotide exchange alters a highly conserved serine residue into arginine (p.Ser108Arg) (Figure 1E). The mutations were not present in public databases, including dbSNP147 (https://www.ncbi.nlm.nih.gov/SNP/), and ExAC (http://exac.broadinstitute.org). Both mutations were predicted to affect function by *in silico* software analysis with combined annotation dependent depletion scores (CADD, http://cadd.gs.washington.edu/) of 35 for the deletion and 24 for the missense variant. Accordingly, both mutations would be predicted to be within the 1 % most deleterious substitutions in the human genome.

The fact that males affected by MEHMO syndrome from three independent families carried the same *EIF2S3* 4 bp deletion prompted us to study their possible relatedness. The families themselves had no knowledge of any common ancestors. Identity by descent (IBD) analysis (see Supplementary Information) using SNP array data from index patients of families 1 and 3 did not reveal any regions on the X chromosome to be identical by descent greater than 0.5 cM, excluding relationships between the affecteds of up to 4th degree cousins with high probability. Subsequent comparison of WES data from index patients of the Slovak families 1 and 2, the mother from family 2, and X-chromosome sequencing data from the index patient from family 3 suggested a founder effect in these three families but with more distant relatedness (Supp. Tables S1 and S2).

No variants were found in the coding and adjacent intronic regions of *EIF2S3* in the index patients described by (Leshinsky-Silver, et al., 2002) and (Delozier-Blanchet, et al., 1989).

MEHMO Syndrome Mutations in Yeast eIF2γ Impair Translation Initiation and Decrease Fidelity of Start Codon Selection

Recent high-resolution cryo-EM images of the yeast 48S PIC have provided insights into the structure of eIF2 and its interactions with other components of the PIC (Hussain, et al., 2014; Llacer, et al., 2015). As shown in Figures 2A,B, the eIF2 ternary complex (TC) docks on the intersubunit face of the 40S subunit with the primary contacts between the TC and the ribosome limited to the Met-tRNA$_i^{Met}$ (green in the figure) and the N-terminal portions of the eIF2α subunit (light yellow). The eIF2γ subunit consists of three domains: an N-terminal GTP-binding (G) domain and two β-barrel domains DII and DIII (Figure 2C,3A). The eIF2β subunit binds to the backside of the G domain (opposite the face that contacts GTP), while eIF2α binds to domain DII. The acceptor arm of Met-tRNA$_i^{Met}$ binds into a groove between the G domain and domains DII and DIII (Figure 2B).

The human eIF2γ-Ile465Serfs*4 mutation lies at the C-terminus of human eIF2γ. While the C-terminus of yeast eIF2γ is not fully resolved in the structure (Figure 2B,C), the corresponding residues, Leu523 (L523) to the C-terminus, lie on the backside of the protein, remote from binding sites for eIF2α, eIF2β, Met-tRNA$_i^{Met}$, and the ribosome. The eIF2γ missense mutation identified in this study, p.Ser108Arg, also lies in a region not fully resolved in the yeast eIF2γ structure. The corresponding residue in yeast eIF2γ is Asp167 (D167), which is in a flexible loop that is part of a zinc-binding ribbon inserted within the G domain (Figure 2C). As the function of the Zn^{2+}-binding element in eIF2γ is unknown and it does not appear to interact with any other components in the 48S PIC (Llacer, et al., 2015), it is currently not possible to predict how the p.Ser108Arg mutation within a flexible loop of the element impacts

eIF2 function. The p.Ile259Met mutation identified in the patient described by Moortgat et al (Moortgat, et al., 2016), lies on the face of domain II that forms the binding cleft for Met-tRNA$_i^{Met}$ (Figure 2B,C). The corresponding residue in yeast eIF2γ is Ile318. Interestingly, mutation of the adjacent conserved Arg319 residue in yeast eIF2γ to Asp was lethal, indicating a critical function for this region of eIF2γ (Roll-Mecak, et al., 2004).

To test if the newly identified *EIF2S3* mutations impair eIF2 function, yeast models of the mutants were generated. To test the impact of the C-terminal mutation on eIF2γ function, a yeast/human (*Sc/Hs*) chimeric form of eIF2γ was generated by replacing the C-terminal 13 residues of yeast eIF2γ (residues 515-527) with the corresponding C-terminal 16 residues of human eIF2γ (residues 457-472) (Figure 3A,B). This fusion point was chosen because, as shown in Figure 3B (and in Supp. Figure S1), human and yeast eIF2γ show strong sequence similarity with identical amino acids at 18 of the last 19 residues preceding the fusion point in the chimera (compare yeast residues Glu497-Trp514 with human residues Glu439-Trp456). In addition to the wild-type chimera (*Sc*$^{1-514}$/*Hs*$^{457-472}$; *Sc/Hs*), the *Sc/Hs-Ile465Serfs*4* mutant was generated by deleting the same four nucleotides deleted in the patients. As shown in Figure 3B, the mutation replaces the eight C-terminal residues of human eIF2γ (-IKPTVDDD) with three novel residues (-SQQ).

Yeast expressing the *Sc/Hs* eIF2γ chimera as the sole form of eIF2γ grew like yeast expressing wild-type yeast eIF2γ with no discernable growth defect at either 30 or 37 °C (Figure 3C). In contrast, yeast expressing the *Sc/Hs-Ile465Serfs*4* mutant exhibited a slight slow growth (Slg$^-$) phenotype at 30 °C that was exacerbated at 37 °C (Figure 3C). The Slg$^-$ phenotype was not due to reduced protein levels as

Western blot analysis of whole cell extracts revealed that both the *Sc/Hs* chimera and the *Sc/Hs-Ile465Serfs*4* mutant were expressed at levels equivalent to wild-type yeast eIF2γ (data not shown). As a positive control in these growth assays, we tested the yeast eIF2γ-Val281Thr and eIF2γ-Val281Lys mutants, corresponding to the human eIF2γ-Ile222Thr mutation in the previously described patients with XLID (Borck, et al., 2012). As observed previously, the Val281Lys mutation conferred a striking Slg$^-$ phenotype (Figure 3C).

To further explore the impact of the eIF2γ C-terminal frameshift mutation on eIF2 function, a *GCN4-lacZ* reporter was introduced into isogenic yeast strains expressing wild-type yeast eIF2γ, the *Sc/Hs* chimera, the chimera with the Ile465Serfs*4 mutation, or, as a positive control, yeast eIF2γ-Val281Thr, which was previously shown to impair eIF2 function and cause derepression of *GCN4* expression (Borck, et al., 2012). Mutations that lower eIF2 activity lead to elevated *GCN4* (yeast homolog of *ATF4*) expression by limiting reinitiation (Hinnebusch, 2005) Thus, ribosomes scanning downstream after translation of the first uORF (uORF1) on the *GCN4* mRNA fail to reinitiate at the inhibitory uORFs 3 and 4 and continue scanning. The added scanning time enables the ribosomes to acquire an eIF2 TC and reinitiate translation at the *GCN4* ORF instead. Whereas *GCN4-lacZ* reporter expression was similarly repressed in yeast expressing wild type eIF2γ or the *Sc/Hs* chimera, the Ile465Serfs*4 mutation derepressed *GCN4* expression nearly 3-fold, comparably to cells expressing eIF2γ-Val281Thr (Figure 4A). These results demonstrate that the C-terminal mutation in eIF2γ impairs eIF2 function to a similar extent as the previously examined eIF2γ-Val281Thr mutation.

In addition to derepressing *GCN4* expression, mutations that impair eIF2 function have also been found to lower the fidelity of translation initiation and enable ribosomes to initiate at non-AUG codons. Whereas translation is normally stringently restricted to initiate at an AUG codon, mutations that weaken Met-tRNA$_i^{Met}$ binding to eIF2, enhance eIF2 GTPase activity, or disrupt eIF2 integrity, enhance initiation at non-AUG codons and confer a suppressor of initiation (Sui$^-$) phenotype in yeast (Hinnebusch, 2011). To assess translation initiation fidelity, *HIS4-lacZ* reporter constructs with an AUG or UUG start codon were introduced into the same strains used to examine *GCN4* expression. Consistent with previous reports, expression of the *HIS4(UUG)-LacZ* reporter was substantially poorer than expression of the *HIS4(AUG)-LacZ* reporter in cells expressing wild-type and *Sc/Hs* chimeric eIF2γ leading to a low UUG/AUG initiation ratio ((Castilho-Valavicius, et al., 1990; Donahue, et al., 1988; Dorris, et al., 1995), and Figure 4B, 1st bar). Consistent with the notion that the eIF2γ-Ile465Serfs*4 mutation impairs eIF2 function, the UUG/AUG ratio was increased ~2-fold in cells expressing this eIF2γ mutant compared to cells expressing the *Sc*/*Hs* chimera (Figure 4B, 2nd and 3rd bar). This 2-fold increase in the UUG/AUG initiation ratio is similar to what was observed in cells expressing the eIF2γ-Val281Thr mutant (Figure 4B, 4th bar). Taken together, these results demonstrate that the C-terminal mutation in eIF2γ impairs eIF2 function.

As stated above, the p.Ser108Arg mutation in human eIF2γ lies in a flexible loop within the putative Zn^{2+}-binding element. Based on sequence alignment of human and yeast eIF2γ (Supp. Figure S1), yeast eIF2γ residue Asp167 corresponds to human eIF2γ residue Ser108. As shown in Figure 3C, yeast expressing eIF2γ-Asp167Arg as the sole source of eIF2γ exhibited no growth defects at either 30 or 37

°C, nor did the mutation affect *GCN4* expression or translation start site selection (UUG initiation; data not shown). Combining the results obtained in yeast with the limited number of family members tested for the variant, we currently interprete the p.Ser108Arg substitution as a variant of unknown significance according to American College of Medical Genetics guidelines (Richards, et al., 2015).

Elevated *DDIT3*/CHOP Expression in MEHMO Patient-Derived Fibroblasts

Given that the 4 bp deletion identified in families 1-3 is located in the last exon of *EIF2S3*, we assumed that the corresponding mutant mRNA would likely not undergo degradation by nonsense-mediated decay and instead would be translated into a truncated protein. To test this, we performed Western blot analysis for endogenous eIF2γ protein using whole cell lysates from patient and control fibroblast cell lines. In all samples with concentrated protein a specific product could be detected, whereas only very faint signals could be obtained without prior protein concentration (Figure 1F). These results demonstrate that eIF2γ is expressed in human fibroblasts as expected given its essential role in cellular protein synthesis, and that the C-terminal truncated protein is produced in the patients. Furthermore, we examined transiently expressed N-terminal (FLAG) and C-terminal (myc) tagged wild-type and mutant eIF2γ proteins in HeLa and HEK293T cells and could detect the proteins using anti-FLAG and anti-myc antibodies (Supp. Figure S2). Next, we investigated the subcellular localization of transiently expressed eIF2γ in HEK293T cells and the results did not reveal any major differences between the wild-type and mutant proteins (Supp. Figure S3).

Having found that the C-terminal frameshift mutation impairs eIF2γ function and derepresses *GCN4* expression in yeast, we investigated whether the ISR is induced in patient-derived fibroblasts. A key control point in the ISR is ATF4. Like its yeast homolog *GCN4*, expression of *ATF4* is controlled by uORFs and both proteins are transcription factors that direct the expression of key stress response proteins. We assessed the transcript level of the ATF4 target gene *DDIT3* by RT-qPCR and the levels of the *DDIT3*-encoded CHOP protein by Western blot in patient and control fibroblast samples. RT-qPCR experiments were performed using RNA extracted from patient IV:1 from family 3 (six biological replicates) and at least four control fibroblasts (three biological replicates) from healthy male individuals. The *DDIT3* transcript level was significantly increased (2.5-fold) in the patient relative to the controls (Figure 5A), and Western blot analysis of whole cell lysates confirmed significantly elevated CHOP protein levels in the patient compared to control fibroblasts (see representative Western blot in Figure 5B).

Discussion

This study demonstrates that mutations in *EIF2S3* encoding the translation initiation factor eIF2γ are associated with the XLID syndrome MEHMO. Since its initial description more than 25 years ago (Delozier-Blanchet, et al., 1989), only five families have been reported with full MEHMO syndrome (including two new families from this study). In three of the families, we have found the C-terminal p.Ile465Serfs mutation. Inspection of sequencing data and haplotype analysis on available family members suggests that the families could be distantly related. An additional family carrying this pathogenic variant has been described very recently (Moortgat, et al.,

2016); however, the phenotype was not described as MEHMO syndrome, probably due to early death of the patient at 12 months. In two families (Delozier-Blanchet, et al., 1989; Leshinsky-Silver, et al., 2002), no mutation was found in the *EIF2S3* gene. While the patient reported by Leshinsky-Silver et al (Leshinsky-Silver, et al., 2002) carried a deleterious (p.Tyr430X) mutation in the *SERAC1* (MIM# 614725) gene, the genetic defect in the family reported by DeLozier-Blanchet (DeLozier-Blanchet, et al., 1999; Delozier-Blanchet, et al., 1989) could be located outside the *EIF2S3* region examined by WES or the disease in this family might have been caused by a mutation in another gene mimicking the MEHMO syndrome.

Interestingly, to date four different mutations have been found in the *EIF2S3* gene in patients described as having syndromic XLID. Phenotypic overlap with MEHMO syndrome is now evident in all cases. All four index patients carrying the C-terminal frameshift mutation presented the full spectrum of MEHMO syndrome including microcephaly, epileptic seizures, hypogonadism, hypogenitalism, and obesity. Moreover, three of the patients developed insulin-dependent diabetes in the first year of life. All of the patients with the frameshift mutation failed to achieve head control, were not able to make any voluntary movements, and did not have any social interactions. In addition, typical facial dysmorphisms were present in these patients. In contrast, the patients with the missense mutations identified to date are less severely affected and present only subsets of symptoms that can differ even within family members carrying the same mutation. For example, the boy reported in this study with the maternally inherited p.Ser108Arg substitution of currently unknown clinical significance does not have diabetes or epilepsy. Moreover, in a family with the p.Ile259Met mutation, epilepsy was present only in one (III:2) of the two affected males. Both patients were able to perform movements and were capable of social

interaction, and one of them even spoke several words (Moortgat, et al., 2016). In our previously published family with the p.Ile222Thr mutation, the patients had only moderate-to-severe ID (one of them can speak in short sentences and feed himself). One of these latter patients lived into adulthood, and they were able to walk (ataxic gait). Other clinical features of MEHMO syndrome were present individually in this family - generalized seizures (patient III:2) and post-pubertal microgenitalism and obesity (patient II:3) (Borck, et al., 2012). The final reported missense mutation p.Val151Leu was found in one XLID family, but further phenotypic information was unavailable (Tarpey, et al., 2009).

Although a larger case series will be required to define genotype-phenotype relations in MEHMO syndrome, the variable clinical severity may depend on the type and localization of the *EIF2S3* mutations with the eIF2γ C-terminal frameshift mutation being more deleterious than the reported amino acid substitutions. We assessed the impact of the mutations found in our patients in a yeast model. Consistent with the more severe patient symptoms, the eIF2γ-Ile465Serfs*4 mutation significantly impaired yeast cell growth (Figure 3), while yeast expressing the eIF2γ-Asp167Arg and eIF2γ-Val281Thr mutants (corresponding to the Ser108Arg and Ile222Thr mutations in human eIF2γ, respectively) grew comparably to the control strain expressing wild-type eIF2γ (Figure 3). Interestingly, measurement of *GCN4* expression and the fidelity of translation start site selection demonstrated that the C-terminal truncating mutation in eIF2γ impairs eIF2 function to a similar extent as the eIF2γ-Val281Thr mutation, while the eIF2γ-Asp167Arg missense mutation did not influence these assays. The lack of observable phenotype for this latter mutation in yeast suggests that the impact of the mutation may be more noticable in multicellular

organisms or that the mutation specifically impairs a function of human eIF2γ that is not shared with the yeast factor.

Pathogenic variants of eIF2γ could impact eIF2 function in various ways including altering the binding of eIF2γ to its counterparts eIF2α and eIF2β, altering the binding of eIF2 to Met-tRNA$_i^{Met}$, GTP, the ribosome or other translation factors, or altering eIF2γ expression or stability. We have shown that the C-terminal frameshift mutation does not result in loss of the eIF2γ protein, suggesting instead that it impairs eIF2 function. In this context it is interesting to note that two mutations causing similar impairments in eIF2 function were previously identified near the C-terminus of yeast eIF2γ. The *gcd11-503* mutant, which generates eIF2γ-Arg510His, derepressed *GCN4* expression and increased initiation at non-AUG codons, while the *gcd11-508* mutant, which causes a frameshift that replaces the C-terminal three residues in yeast eIF2γ (normally –PIA, see Supp. Figure S1) with the sequence –VGIEINYHLLTSYITSILSYTVLEDDANDEK, derepressed *GCN4* expression, but did not lessen the fidelity of translation start site selection (Dorris, et al., 1995). Thus, an intact C-terminus is critical for proper eIF2 function *in vivo,* although the precise molecular role remains to be determined. The remaining eIF2γ mutations linked to XLID are located in distinct regions of the protein. As reported previously (Borck, et al., 2012), the Ile222Thr mutation in human eIF2γ, corresponding to the residue Val281 in *Saccharomyces cerevisiae* eIF2γ (Figure 3A and Supp. Figure S1), lies in the docking site for helix α1 of eIF2β (Figure 2B) and mutation of this residue impaired the binding of eIF2β to both yeast and human eIF2γ. The recently identified p.Ile259Met mutation (Moortgat, et al., 2016) (Ile318 in yeast) lies near the Met-tRNA$_i^{Met}$ binding site and mutation of the adjacent Arg319 to Asp in yeast eIF2γ was

lethal (Roll-Mecak, et al., 2004). Neither the C-terminal frameshift mutation nor the novel p.Ser108Arg variant are localized in functionally defined regions of eIF2γ and their exact functional consequences are hard to predict.

In mammals and other metazoans, down-regulation of eIF2 function through phosphorylation of eIF2α activates the ISR (Harding, et al., 2003), which corresponds to the translational arm of the UPR. As originally observed for the *GCN4* mRNA in yeast (Hinnebusch, 2005), regulated reinitiation at uORFs governs the translation of the *ATF4* mRNA in a manner controlled by eIF2 function (Harding, et al., 2000; Lu, et al., 2004; Vattem, et al., 2004; Young, et al., 2016). We confirmed in patient-derived fibroblasts that the C-terminal eIF2γ frameshift mutation leads to activation of the ISR, consistent with the notion that the mutation lowers eIF2 function. Increased expression of *DDIT3* and its corresponding protein CHOP show that MEHMO syndrome belongs to the group of disorders caused by dysregulation of translation or the UPR (Table 3). Moreover, the clinical picture of MEHMO syndrome shares common features with these disorders. Mutations in eIF2γ, like mutations in *EIF2B1* (MIM# 606686), *EIF2B2* (MIM# 606454), *EIF2B3* (MIM# 606273), *EIF2B4* (MIM# 606687), *EIF2B5* (MIM# 603945), and *PPP1R15B* (MIM# 613257), impair the activity or availability of TC. This could lead to a general insufficiency of protein synthesis that most significantly impacts processes requiring high rates of protein synthesis and will also cause increased sensitivity in states of elevated metabolic requirements. Moreover, the decreased translation rate and attendant chronically elevated ATF4 and CHOP levels result in apoptosis (Han, et al., 2013; Matsumoto, et al., 2013; Tabas, et al., 2011; Walter, et al., 2011). In vanishing white matter (VWM) disease (MIM# 603896) caused by mutations in any of the subunits of eIF2B,

mutated cells are hypersensitive to stressors that lead to eIF2α phosphorylation (Kantor, et al., 2005; van der Voorn, et al., 2005). Similarly, patients with VWM syndrome can undergo rapid deterioration following stress such as fever, minor head trauma, or even fright (Labauge, et al., 2009; Schiffmann, et al., 1994; Vermeulen, et al., 2005). Like the VWM patients, the condition of Patient 1 in our study was markedly aggravated during periods of illness. Interestingly, the VWM syndrome pathology is mainly localized to the brain and ovaries, while MEHMO syndrome is more generalized (though the white matter changes are reminiscent of VWM). In contrast, patients with mutations in *PPP1R15B* share additional symptoms with the *EIF2S3* male mutation carriers including diabetes, severe microcephaly, growth retardation, developmental delay, ID and bone dysplasia (Abdulkarim, et al., 2015; Kernohan, et al., 2015).

In contrast to diseases like VWM and MEHMO syndrome, which are linked to induction of the ISR or UPR, insufficient activation of the UPR is also linked to disease. In Wolcott-Rallison syndrome (WRS) (MIM# 226980), mutated PERK (encoded by *EIF2AK3,* MIM# 604032) fails to phosphorylate eIF2α in response to ER stress. This results in impaired down-regulation of protein synthesis and further ER overload (Harding, et al., 2001; Volchuk, et al., 2010). The UPR is important for proliferation and differentiation of pancreatic β-cells (Kaufman, et al., 2010; Zhang, et al., 2006), and dedifferentiation from a secretory phenotype in chondrocytes may play a role in adaptation to chronic stress (Rajpar, et al., 2009; Tsang, et al., 2007). The dysregulation of the UPR may thus explain the main features of WRS – permanent neonatal diabetes and epiphyseal dysplasia. Despite their different impacts on the UPR, another frequent symptom of WRS – episodes of acute liver failure triggered by intercurrent diseases such as upper airway infections (Julier, et

al., 2010) – is similar to the progressive deterioration in MEHMO and VWM syndromes. Moreover, MEHMO Patient 3 (this report) had congenital scoliosis, a feature commonly associated with WRS.

In addition to the PERK mutations that cause WRS by altering ER homeostasis, ER proteins that likewise play a role in ER homeostasis and correct protein folding were found to be mutated in syndromes with clinical features that overlap MEHMO syndrome. For example, mutations in *DNAJC3* (MIM# 601184) (Synofzik, et al., 2014), *SIL1* (MIM# 608005) (Senderek, et al., 2005), *WFS1* (MIM# 606201) (Fonseca, et al., 2005), and *IER3IP1* (MIM# 609382) (Abdel-Salam, et al., 2012) (Table 3, Figure 6) result in accumulation of misfolded proteins in the ER leading to UPR activation. The MEDS syndrome (MIM# 614231) caused by *IER3IP1* mutations strikingly resembles MEHMO syndrome with affected patients suffering from severe developmental delay, seizures difficult to control, insulin dependent diabetes, and hypotonia. Moreover, some MEDS syndrome patients were obese and one had hypogonadism. The facial features of MEDS syndrome patients are also similar to MEHMO patients with full cheeks and large ears. In addition to these similarities with MEHMO syndrome, some MEDS patients shared features with WRS syndrome including skeletal abnormalities and repeated bone fractures. The function of IER3IP1 protein is not fully understood, but the protein seems to play a role in maintaining vesicular trafficking between the ER and Golgi, and cells with non-functional IER3IP1 are more susceptible to cellular stress and subsequent apoptosis (Poulton, et al., 2011).

Mutations in other components of the translation apparatus as well as regulators of translation can also cause human disease. We and others showed that mutations in *FTSJ1* (MIM# 300499), *TRMT1* (MIM# 611669), and *NSUN2* (MIM# 610916), which

are implicated in tRNA modification, are associated with ID (MIM# 309549, MIM# 611091) (Abbasi-Moheb, et al., 2012; Davarniya, et al., 2015; Freude, et al., 2004; Guy, et al., 2015; Khan, et al., 2012). Similarly, mutations in *LAS1L* (MIM# 300964), which is important for the biogenesis of the 60S ribosomal subunit, are associated with Wilson-Turner syndrome (MIM# 309585) characterized by obesity, gynecomastia, speech difficulties, emotional lability, tapering fingers, and small feet (Hu, et al., 2016). Finally, mutations in the X-linked *RPL10* gene (MIM# 312173), which codes for a highly conserved multifunctional component of the large 60S ribosomal subunit, are associated with a variable phenotype with XLID or normal cognitive function (MIM# 300847) (Brooks, et al., 2014; Chiocchetti, et al., 2011; Klauck, et al., 2006; Thevenon, et al., 2015; Zanni, et al., 2015).

In brief, the clinical symptoms associated with mutations in eIF2γ (MEHMO syndrome), eIF2B (childhood ataxia with central nervous system hypomyelinization (CACH)/VWM syndrome) and *PPP1R15B* which encodes CReP indicate that sustained low-level protein synthesis is poorly tolerated. At the same time, the overlapping phenotypes in WRS result from impaired downregulation of translation in response to a variety of stress conditions. Thus, tight regulation of protein synthesis and its adaptation to cellular stress are critical for health and for development. Moreover, the lack of appropriate regulation helps to explain the significant influence of environment that can modulate the course and severity of these diseases.

In conclusion, this study establishes the link between mutations in the *EIF2S3* gene and MEHMO syndrome. Our findings contribute to an increasing list of disorders caused by dysregulation of protein synthesis and underscore the importance of considering genes involved in translation and its regulation as candidates for ID associated syndromes.

Acknowledgments

We are indebted to the families of our patients and primary care physicians for their cooperation in this study. This work was supported in part by research grants of the DIABGENE Laboratory funded by the Scientific Grant Agency of the Ministry of Education, Science, Research and Sport of the Slovak Republic (2/0166/14), by the Slovak Research and Development Agency (APVV-187-12), by Transendogen (26240220051), which is supported by the Research & Development Operational Programme and by the ERDF, by the intramural research program of the National Institutes of Health, and by the EU FP7 project GENCODYS, grant number 241995. L.H. was supported by the John and Patricia Farrant Scholarship and an Australian Postgraduate Award Scholarship. M.B. was supported by an NHMRC Senior Research Fellowship (APP1102971) and NHMRC Program Grant (APP1054618). This work was also supported by Victorian State Government Operational Infrastructure Support, Australian Government NHMRC IRIISS funding. The authors declare that they have no conflict of interest.

References

Abbasi-Moheb L, Mertel S, Gonsior M, Nouri-Vahid L, Kahrizi K, Cirak S, Wieczorek D, Motazacker MM, Esmaeeli-Nieh S, Cremer K, Weissmann R, Tzschach A,

et al. 2012. Mutations in NSUN2 cause autosomal-recessive intellectual disability. Am J Hum Genet 90(5):847-55.

Abdel-Salam GM, Schaffer AE, Zaki MS, Dixon-Salazar T, Mostafa IS, Afifi HH, Gleeson JG. 2012. A homozygous IER3IP1 mutation causes microcephaly with simplified gyral pattern, epilepsy, and permanent neonatal diabetes syndrome (MEDS). Am J Med Genet A 158A(11):2788-96.

Abdulkarim B, Nicolino M, Igoillo-Esteve M, Daures M, Romero S, Philippi A, Senee V, Lopes M, Cunha DA, Harding HP, Derbois C, Bendelac N, et al. 2015. A Missense Mutation in PPP1R15B Causes a Syndrome Including Diabetes, Short Stature, and Microcephaly. Diabetes 64(11):3951-62.

Alone PV, Cao C, Dever TE. 2008. Translation initiation factor 2gamma mutant alters start codon selection independent of Met-tRNA binding. Mol Cell Biol 28(22):6877-88.

Bahlo M, Bromhead CJ. 2009. Generating linkage mapping files from Affymetrix SNP chip data. Bioinformatics 25(15):1961-2.

Boeke JD, Trueheart J, Natsoulis G, Fink GR. 1987. 5-Fluoroorotic acid as a selective agent in yeast molecular genetics. Methods Enzymol 154:164-75.

Borck G, Shin BS, Stiller B, Mimouni-Bloch A, Thiele H, Kim JR, Thakur M, Skinner C, Aschenbach L, Smirin-Yosef P, Har-Zahav A, Nurnberg G, et al. 2012. eIF2gamma mutation that disrupts eIF2 complex integrity links intellectual disability to impaired translation initiation. Mol Cell 48(4):641-6.

Brooks SS, Wall AL, Golzio C, Reid DW, Kondyles A, Willer JR, Botti C, Nicchitta CV, Katsanis N, Davis EE. 2014. A novel ribosomopathy caused by dysfunction of RPL10 disrupts neurodevelopment and causes X-linked microcephaly in humans. Genetics 198(2):723-33.

Castilho-Valavicius B, Yoon H, Donahue TF. 1990. Genetic characterization of the Saccharomyces cerevisiae translational initiation suppressors sui1, sui2 and SUI3 and their effects on HIS4 expression. Genetics 124(3):483-95.

Chiocchetti A, Pakalapati G, Duketis E, Wiemann S, Poustka A, Poustka F, Klauck SM. 2011. Mutation and expression analyses of the ribosomal protein gene RPL10 in an extended German sample of patients with autism spectrum disorder. Am J Med Genet A 155A(6):1472-5.

Cigan AM, Pabich EK, Donahue TF. 1988. Mutational analysis of the HIS4 translational initiator region in Saccharomyces cerevisiae. Mol Cell Biol 8(7):2964-75.

Davarniya B, Hu H, Kahrizi K, Musante L, Fattahi Z, Hosseini M, Maqsoud F, Farajollahi R, Wienker TF, Ropers HH, Najmabadi H. 2015. The Role of a Novel TRMT1 Gene Mutation and Rare GRM1 Gene Defect in Intellectual Disability in Two Azeri Families. PLoS One 10(8):e0129631.

DeLozier-Blanchet CD, Haenggeli CA, Bottani A. 1999. MEHMO, a novel syndrome: assignment of disease locus to Xp21.1-p22.13. Mental retardation, epileptic seizures, hypogonadism and genitalism, microcephaly, obesity. Eur J Hum Genet 7(6):621-2.

Delozier-Blanchet CD, Haenggeli CA, Engel E. 1989. [Microencephalic nanism, severe retardation, hypertonia, obesity, and hypogonadism in two brothers: a new syndrome?]. J Genet Hum 37(4-5):353-65.

Dever TE. 2002. Gene-specific regulation by general translation factors. Cell 108(4):545-56.

Dever TE. 2007. The eIF2α kinases. In: Mathews MB, Sonenberg N, Hershey JWB, editors. Translational Control in Biology and Medicine. Cold Spring Harbor, New York: Cold Spring Harbor Laboratory Press. p 319-344.

Donahue TF, Cigan AM. 1988. Genetic selection for mutations that reduce or abolish ribosomal recognition of the HIS4 translational initiator region. Mol Cell Biol 8(7):2955-63.

Dorris DR, Erickson FL, Hannig EM. 1995. Mutations in GCD11, the structural gene for eIF-2 gamma in yeast, alter translational regulation of GCN4 and the selection of the start site for protein synthesis. EMBO J 14(10):2239-49.

Emde AK, Schulz MH, Weese D, Sun R, Vingron M, Kalscheuer VM, Haas SA, Reinert K. 2012. Detecting genomic indel variants with exact breakpoints in single- and paired-end sequencing data using SplazerS. Bioinformatics 28(5):619-27.

Fonseca SG, Fukuma M, Lipson KL, Nguyen LX, Allen JR, Oka Y, Urano F. 2005. WFS1 is a novel component of the unfolded protein response and maintains homeostasis of the endoplasmic reticulum in pancreatic beta-cells. J Biol Chem 280(47):39609-15.

Freude K, Hoffmann K, Jensen LR, Delatycki MB, des Portes V, Moser B, Hamel B, van Bokhoven H, Moraine C, Fryns JP, Chelly J, Gecz J, et al. 2004. Mutations in the FTSJ1 gene coding for a novel S-adenosylmethionine-binding protein cause nonsyndromic X-linked mental retardation. Am J Hum Genet 75(2):305-9.

Guy MP, Shaw M, Weiner CL, Hobson L, Stark Z, Rose K, Kalscheuer VM, Gecz J, Phizicky EM. 2015. Defects in tRNA Anticodon Loop 2'-O-Methylation Are

Implicated in Nonsyndromic X-Linked Intellectual Disability due to Mutations in FTSJ1. Hum Mutat 36(12):1176-87.

Han J, Back SH, Hur J, Lin YH, Gildersleeve R, Shan J, Yuan CL, Krokowski D, Wang S, Hatzoglou M, Kilberg MS, Sartor MA, et al. 2013. ER-stress-induced transcriptional regulation increases protein synthesis leading to cell death. Nat Cell Biol 15(5):481-90.

Harding HP, Novoa I, Zhang Y, Zeng H, Wek R, Schapira M, Ron D. 2000. Regulated translation initiation controls stress-induced gene expression in mammalian cells. Mol Cell 6(5):1099-108.

Harding HP, Zeng H, Zhang Y, Jungries R, Chung P, Plesken H, Sabatini DD, Ron D. 2001. Diabetes mellitus and exocrine pancreatic dysfunction in perk-/- mice reveals a role for translational control in secretory cell survival. Mol Cell 7(6):1153-63.

Harding HP, Zhang Y, Zeng H, Novoa I, Lu PD, Calfon M, Sadri N, Yun C, Popko B, Paules R, Stojdl DF, Bell JC, et al. 2003. An integrated stress response regulates amino acid metabolism and resistance to oxidative stress. Mol Cell 11(3):619-33.

Henden L, Wakeham D, Bahlo M. 2016. XIBD: software for inferring pairwise identity by descent on the X chromosome. Bioinformatics 32(15):2389-91.

Hinnebusch AG. 1985. A hierarchy of trans-acting factors modulates translation of an activator of amino acid biosynthetic genes in Saccharomyces cerevisiae. Mol Cell Biol 5(9):2349-60.

Hinnebusch AG. 2005. Translational regulation of GCN4 and the general amino acid control of yeast. Annu Rev Microbiol 59:407-50.

Hinnebusch AG. 2011. Molecular mechanism of scanning and start codon selection in eukaryotes. Microbiol Mol Biol Rev 75(3):434-67, first page of table of contents.

Hinnebusch AG. 2014. The scanning mechanism of eukaryotic translation initiation. Annu Rev Biochem 83:779-812.

Hu H, Haas SA, Chelly J, Van Esch H, Raynaud M, de Brouwer AP, Weinert S, Froyen G, Frints SG, Laumonnier F, Zemojtel T, Love MI, et al. 2016. X-exome sequencing of 405 unresolved families identifies seven novel intellectual disability genes. Mol Psychiatry 21(1):133-48.

Hussain T, Llacer JL, Fernandez IS, Munoz A, Martin-Marcos P, Savva CG, Lorsch JR, Hinnebusch AG, Ramakrishnan V. 2014. Structural changes enable start codon recognition by the eukaryotic translation initiation complex. Cell 159(3):597-607.

Julier C, Nicolino M. 2010. Wolcott-Rallison syndrome. Orphanet J Rare Dis 5:29.

Kantor L, Harding HP, Ron D, Schiffmann R, Kaneski CR, Kimball SR, Elroy-Stein O. 2005. Heightened stress response in primary fibroblasts expressing mutant eIF2B genes from CACH/VWM leukodystrophy patients. Hum Genet 118(1):99-106.

Kaufman RJ, Back SH, Song B, Han J, Hassler J. 2010. The unfolded protein response is required to maintain the integrity of the endoplasmic reticulum, prevent oxidative stress and preserve differentiation in beta-cells. Diabetes Obes Metab 12 Suppl 2:99-107.

Kernohan KD, Tetreault M, Liwak-Muir U, Geraghty MT, Qin W, Venkateswaran S, Davila J, Care4Rare Canada C, Holcik M, Majewski J, Richer J, Boycott KM. 2015. Homozygous mutation in the eukaryotic translation initiation factor

2alpha phosphatase gene, PPP1R15B, is associated with severe microcephaly, short stature and intellectual disability. Hum Mol Genet 24(22):6293-300.

Khan MA, Rafiq MA, Noor A, Hussain S, Flores JV, Rupp V, Vincent AK, Malli R, Ali G, Khan FS, Ishak GE, Doherty D, et al. 2012. Mutation in NSUN2, which encodes an RNA methyltransferase, causes autosomal-recessive intellectual disability. Am J Hum Genet 90(5):856-63.

Kircher M, Witten DM, Jain P, O'Roak BJ, Cooper GM, Shendure J. 2014. A general framework for estimating the relative pathogenicity of human genetic variants. Nat Genet 46(3):310-5.

Klauck SM, Felder B, Kolb-Kokocinski A, Schuster C, Chiocchetti A, Schupp I, Wellenreuther R, Schmotzer G, Poustka F, Breitenbach-Koller L, Poustka A. 2006. Mutations in the ribosomal protein gene RPL10 suggest a novel modulating disease mechanism for autism. Mol Psychiatry 11(12):1073-84.

Labauge P, Horzinski L, Ayrignac X, Blanc P, Vukusic S, Rodriguez D, Mauguiere F, Peter L, Goizet C, Bouhour F, Denier C, Confavreux C, et al. 2009. Natural history of adult-onset eIF2B-related disorders: a multi-centric survey of 16 cases. Brain 132(Pt 8):2161-9.

Larsen S, Kraunsoe R, Gram M, Gnaiger E, Helge JW, Dela F. 2014. The best approach: homogenization or manual permeabilization of human skeletal muscle fibers for respirometry? Anal Biochem 446:64-8.

Leshinsky-Silver E, Zinger A, Bibi CN, Barash V, Sadeh M, Lev D, Sagie TL. 2002. MEHMO (Mental retardation, Epileptic seizures, Hypogenitalism, Microcephaly, Obesity): a new X-linked mitochondrial disorder. Eur J Hum Genet 10(4):226-30.

Llacer JL, Hussain T, Marler L, Aitken CE, Thakur A, Lorsch JR, Hinnebusch AG, Ramakrishnan V. 2015. Conformational Differences between Open and Closed States of the Eukaryotic Translation Initiation Complex. Mol Cell 59(3):399-412.

Lu PD, Harding HP, Ron D. 2004. Translation reinitiation at alternative open reading frames regulates gene expression in an integrated stress response. J Cell Biol 167(1):27-33.

Matsumoto H, Miyazaki S, Matsuyama S, Takeda M, Kawano M, Nakagawa H, Nishimura K, Matsuo S. 2013. Selection of autophagy or apoptosis in cells exposed to ER-stress depends on ATF4 expression pattern with or without CHOP expression. Biol Open 2(10):1084-90.

McWilliam H, Li W, Uludag M, Squizzato S, Park YM, Buso N, Cowley AP, Lopez R. 2013. Analysis Tool Web Services from the EMBL-EBI. Nucleic Acids Res 41(Web Server issue):W597-600.

Moortgat S, Desir J, Benoit V, Boulanger S, Pendeville H, Nassogne MC, Lederer D, Maystadt I. 2016. Two novel EIF2S3 mutations associated with syndromic intellectual disability with severe microcephaly, growth retardation, and epilepsy. Am J Med Genet A 170(11):2927-33.

Pavitt GD, Ron D. 2012. New insights into translational regulation in the endoplasmic reticulum unfolded protein response. Cold Spring Harb Perspect Biol 4(6).

Pesta D, Gnaiger E. 2012. High-resolution respirometry: OXPHOS protocols for human cells and permeabilized fibers from small biopsies of human muscle. Methods Mol Biol 810:25-58.

Poulton CJ, Schot R, Kia SK, Jones M, Verheijen FW, Venselaar H, de Wit MC, de Graaff E, Bertoli-Avella AM, Mancini GM. 2011. Microcephaly with simplified

gyration, epilepsy, and infantile diabetes linked to inappropriate apoptosis of neural progenitors. Am J Hum Genet 89(2):265-76.

Rajpar MH, McDermott B, Kung L, Eardley R, Knowles L, Heeran M, Thornton DJ, Wilson R, Bateman JF, Poulsom R, Arvan P, Kadler KE, et al. 2009. Targeted induction of endoplasmic reticulum stress induces cartilage pathology. PLoS Genet 5(10):e1000691.

Richards S, Aziz N, Bale S, Bick D, Das S, Gastier-Foster J, Grody WW, Hegde M, Lyon E, Spector E, Voelkerding K, Rehm HL, et al. 2015. Standards and guidelines for the interpretation of sequence variants: a joint consensus recommendation of the American College of Medical Genetics and Genomics and the Association for Molecular Pathology. Genet Med 17(5):405-24.

Roll-Mecak A, Alone P, Cao C, Dever TE, Burley SK. 2004. X-ray structure of translation initiation factor eIF2gamma: implications for tRNA and eIF2alpha binding. J Biol Chem 279(11):10634-42.

Ron D, Walter P. 2007. Signal integration in the endoplasmic reticulum unfolded protein response. Nat Rev Mol Cell Biol 8(7):519-29.

Schiffmann R, Moller JR, Trapp BD, Shih HH, Farrer RG, Katz DA, Alger JR, Parker CC, Hauer PE, Kaneski CR, et al. 1994. Childhood ataxia with diffuse central nervous system hypomyelination. Ann Neurol 35(3):331-40.

Senderek J, Krieger M, Stendel C, Bergmann C, Moser M, Breitbach-Faller N, Rudnik-Schoneborn S, Blaschek A, Wolf NI, Harting I, North K, Smith J, et al. 2005. Mutations in SIL1 cause Marinesco-Sjogren syndrome, a cerebellar ataxia with cataract and myopathy. Nat Genet 37(12):1312-4.

Steinmuller R, Steinberger D, Muller U. 1998. MEHMO (mental retardation, epileptic seizures, hypogonadism and -genitalism, microcephaly, obesity), a novel

syndrome: assignment of disease locus to xp21.1-p22.13. Eur J Hum Genet 6(3):201-6.

Su N, Kilberg MS. 2008. C/EBP homology protein (CHOP) interacts with activating transcription factor 4 (ATF4) and negatively regulates the stress-dependent induction of the asparagine synthetase gene. J Biol Chem 283(50):35106-17.

Synofzik M, Haack TB, Kopajtich R, Gorza M, Rapaport D, Greiner M, Schonfeld C, Freiberg C, Schorr S, Holl RW, Gonzalez MA, Fritsche A, et al. 2014. Absence of BiP co-chaperone DNAJC3 causes diabetes mellitus and multisystemic neurodegeneration. Am J Hum Genet 95(6):689-97.

Tabas I, Ron D. 2011. Integrating the mechanisms of apoptosis induced by endoplasmic reticulum stress. Nat Cell Biol 13(3):184-90.

Tarpey PS, Smith R, Pleasance E, Whibley A, Edkins S, Hardy C, O'Meara S, Latimer C, Dicks E, Menzies A, Stephens P, Blow M, et al. 2009. A systematic, large-scale resequencing screen of X-chromosome coding exons in mental retardation. Nat Genet 41(5):535-43.

Thevenon J, Michot C, Bole C, Nitschke P, Nizon M, Faivre L, Munnich A, Lyonnet S, Bonnefont JP, Portes VD, Amiel J. 2015. RPL10 mutation segregating in a family with X-linked syndromic Intellectual Disability. Am J Med Genet A 167A(8):1908-12.

Tsang KY, Chan D, Cheslett D, Chan WC, So CL, Melhado IG, Chan TW, Kwan KM, Hunziker EB, Yamada Y, Bateman JF, Cheung KM, et al. 2007. Surviving endoplasmic reticulum stress is coupled to altered chondrocyte differentiation and function. PLoS Biol 5(3):e44.

van der Voorn JP, van Kollenburg B, Bertrand G, Van Haren K, Scheper GC, Powers JM, van der Knaap MS. 2005. The unfolded protein response in vanishing white matter disease. J Neuropathol Exp Neurol 64(9):770-5.

Vattem KM, Wek RC. 2004. Reinitiation involving upstream ORFs regulates ATF4 mRNA translation in mammalian cells. Proc Natl Acad Sci U S A 101(31):11269-74.

Vermeulen G, Seidl R, Mercimek-Mahmutoglu S, Rotteveel JJ, Scheper GC, van der Knaap MS. 2005. Fright is a provoking factor in vanishing white matter disease. Ann Neurol 57(4):560-3.

Volchuk A, Ron D. 2010. The endoplasmic reticulum stress response in the pancreatic beta-cell. Diabetes Obes Metab 12 Suppl 2:48-57.

Walter P, Ron D. 2011. The unfolded protein response: from stress pathway to homeostatic regulation. Science 334(6059):1081-6.

Young SK, Wek RC. 2016. Upstream Open Reading Frames Differentially Regulate Gene-specific Translation in the Integrated Stress Response. J Biol Chem 291(33):16927-35.

Zanni G, Kalscheuer VM, Friedrich A, Barresi S, Alfieri P, Di Capua M, Haas SA, Piccini G, Karl T, Klauck SM, Bellacchio E, Emma F, et al. 2015. A Novel Mutation in RPL10 (Ribosomal Protein L10) Causes X-Linked Intellectual Disability, Cerebellar Hypoplasia, and Spondylo-Epiphyseal Dysplasia. Hum Mutat 36(12):1155-8.

Zhang W, Feng D, Li Y, Iida K, McGrath B, Cavener DR. 2006. PERK EIF2AK3 control of pancreatic beta cell differentiation and proliferation is required for postnatal glucose homeostasis. Cell Metab 4(6):491-7.

Figure 1. Co-segregating Truncating and Missense Mutations in *EIF2S3* Cause MEHMO Syndrome.

A: Pedigrees of families 1-4 with co-segregating truncating and missense mutations in *EIF2S3*. Open circles represent females, open squares represent unaffected males, closed squares represent affected males, * = mutation carrier, wt = wild-type.

B: Physical appearance of index patient from family 1 at 10 months - obese with full cheeks, large ears, downturned corners of mouth, epiblepharon, long eyelashes and thick eyebrows, tapered fingers and talipes. Microgenitalism is visible.

C: Cranial MRI - Patient 1 – (left) Sagittal T1W image at 4 months showing thin and flat corpus callosum (arrow), and (right) axial T2W image at 19 months showing cerebral atrophy, delay of myelination, acute demyelinating changes in the periventricular white matter, enlarged ventricular system and subarachnoid fronto-temporal space. Patient 2 – (left) T1W image at 10 months showing cerebral atrophy and thin corpus callosum (arrow), and (right) axial T2W image showing enlargement of ventricular system, delay of myelination, and acute demyelinating changes in the periventricular white matter.

D: Electron microscopy of patient 1 muscle biopsy shows myofilament degradation (left) and presence of huge mitochondria with abnormal cristae arrangement (right, arrows).

E: Clustal Omega analysis of eIF2γ C-terminus (left) and the mutated serine residue (right) in humans and other species. The C-terminus is conserved in vertebrates, the Ser108 is conserved down to *Drosophila melanogaster*.

F: Western blot analysis of protein cell lysate from control and patient fibroblast cell lines immunoblotted with anti-eIF2γ antibody shows the presence of eIFγ protein. I = Input, C = concentrated protein.

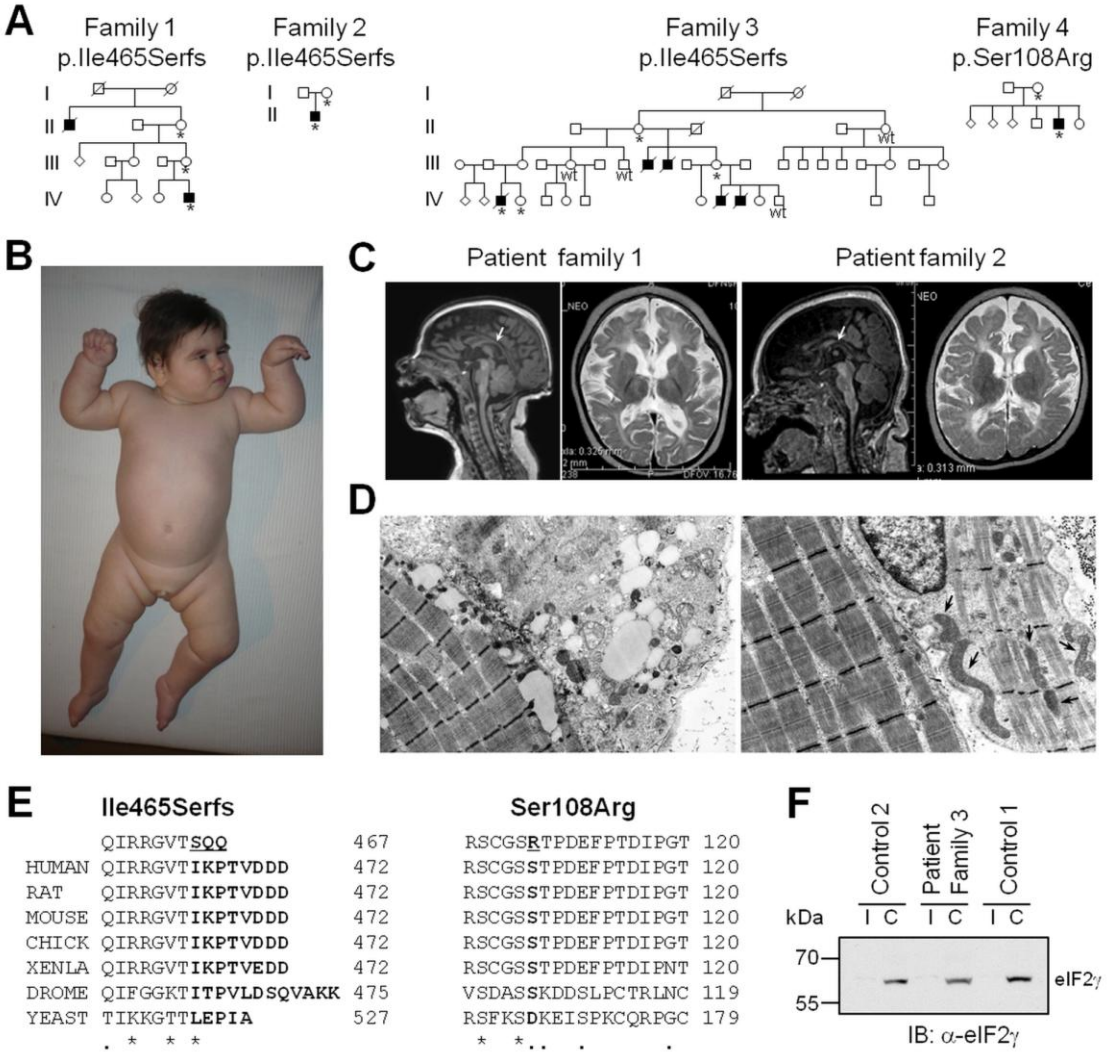

Figure 2. Mutations Map to Distinct Regions of The eIF2γ Structure

A: Ribbons representation of the yeast 48S preinitiation complex (PIC; pdb 3JAP). Only the 18S rRNA of the 40S subunit (gray), Met-tRNA$_i^{Met}$ (green), eIF2α (N-terminal domains, light yellow; C-terminal domain, yellow), eIF2β (helix α1, blue; C-terminal domain, slate) and eIF2γ (cyan) are depicted.

B: Image from panel A rotated as shown and zoomed to highlight the eIF2γ subunit. Sites of the four human mutations are highlighted: S108R (*Sc* D167; red), I222T (*Sc* V281; purple), I259M (*Sc* I318; blue), and I465Sfs*4 (*Sc* L523–C-terminus; orange).

C: Zoom of eIF2γ from panel B. The other eIF2 subunits and 48S complex components have been removed for clarity. Sites of eIF2γ mutations are colored as in panel B and labeled.

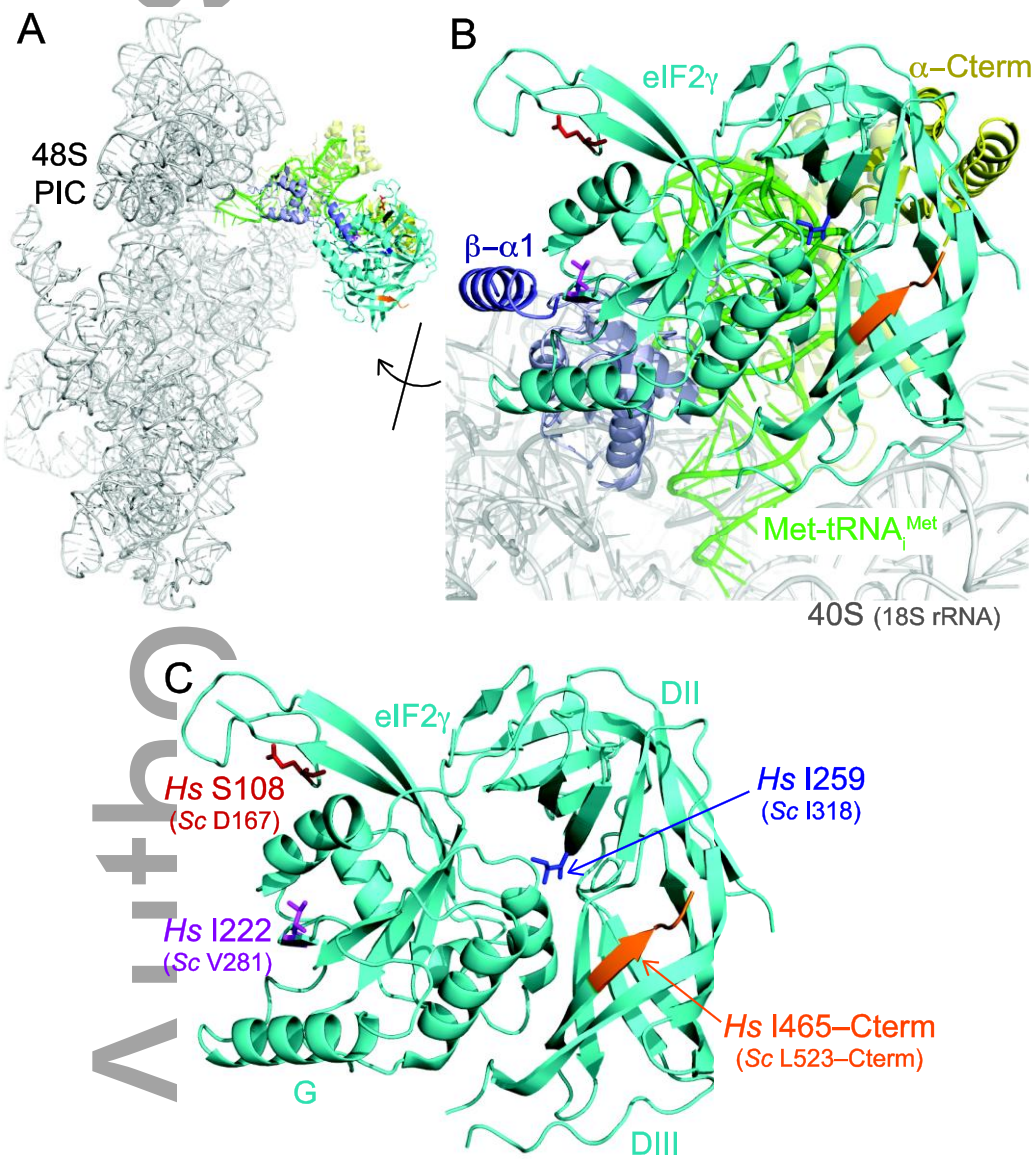

Figure 3. Impact of Mutations in Yeast eIF2γ on Cell Growth

A: Schematics of human (top, brown) and yeast (*Saccharomyces cerevisiae*, Sc, bottom, cyan) eIF2γ highlighting the N-terminal extensions (N), G domains and domains DII and DIII. Sites of mutations in human eIF2γ and the corresponding residues in yeast eIF2γ are labeled and colored as in Figure 2.

B: Alignments (top) of the C-terminal sequences of human (*Hs*, brown) and yeast (*Sc*, cyan) eIF2γ and (bottom) of a yeast/human eIF2γ chimera with either the native human C-terminus (*Sc*/*Hs*) or with the C-terminal frameshift mutation (*Sc*/*Hs-I465Sfs*4*).

C: Serial dilutions of yeast cells expressing, as the sole-source of eIF2γ, the indicated eIF2γ mutants were grown on minimal synthetic dextrose (SD) medium at 30 or 37 °C for 3 days.

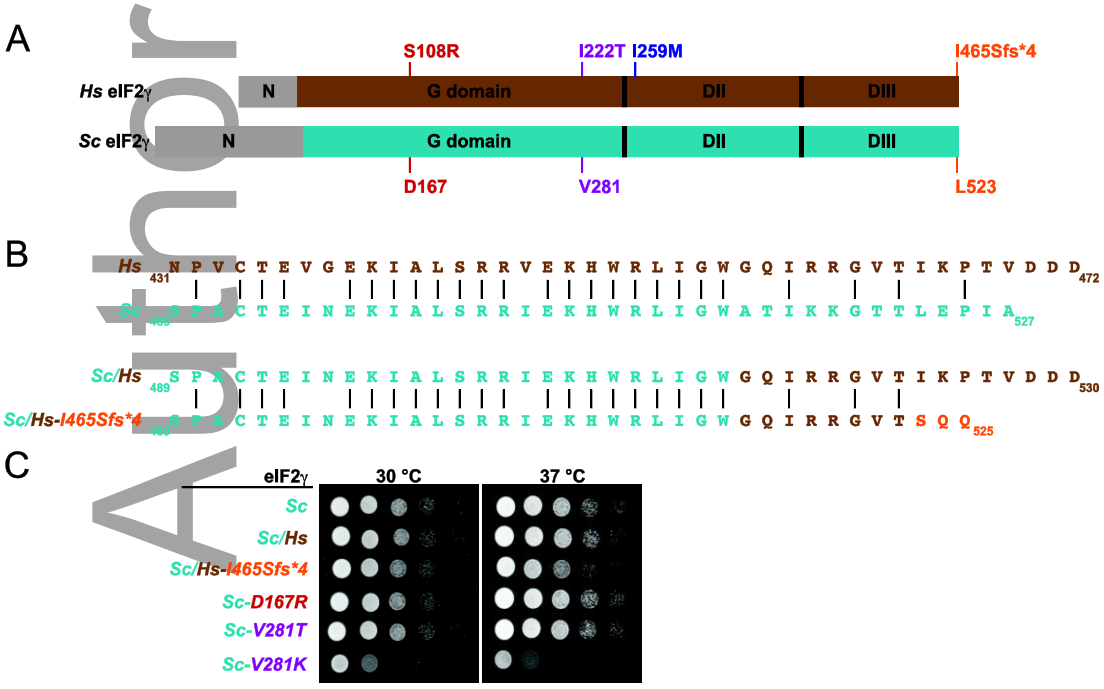

Figure 4. Mutations in Yeast eIF2γ Impair Translation Initiation

A, B: A *GCN4-lacZ* (A) or *HIS4(AUG)* or *HIS4(UUG)* (B) reporter construct was introduced into yeast strains expressing the indicated WT or mutant form of yeast (*Sc*) or of yeast/human chimera (*Sc*/*Hs*) eIF2γ. β-galactosidase activities (A) or mean ratios of activities (B) and standard deviations were determined from at least three independent transformants. The data were assessed by student's t-test and P-values relative to wild-type (*Sc*) eIF2γ (** $P \leq 0.01$, *** $P \leq 0.001$).

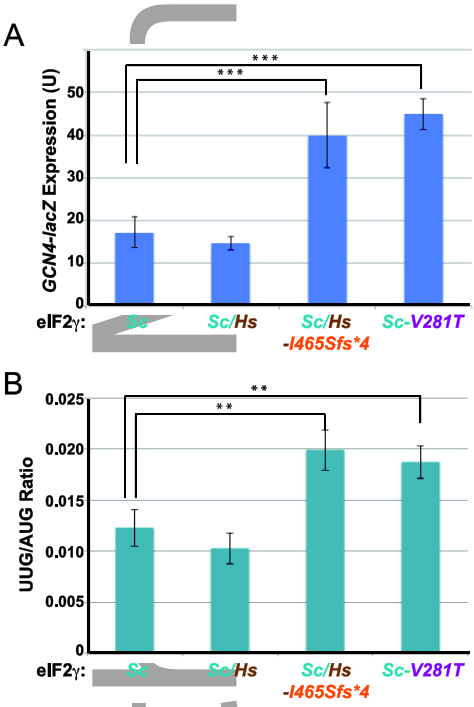

Figure 5. The EIF2S3 C-terminal Mutation is Associated with Elevated *DDIT3/CHOP* Transcript and Protein Levels in Patient Fibroblasts

A: Expression of *DDIT3* mRNA in patient and control fibroblasts measured using RT-qPCR. Levels are normalized to the control and expressed as 2^{-dCq} with SD. *** *P*

<0.001, t-test. Patient fibroblasts show an increased *DDIT3* transcript level compared to controls.

B: Representative Western blot analysis of protein lysates from patient fibroblasts (index from family 3) with C-terminal deleted EIF2S3 and three controls. Whole cell lysate from patient and control fibroblasts was concentrated and separated on SDS-PAGE. The gel was blotted and probed with an anti-CHOP antibody (upper panel). The blot was subsequently probed with an anti-tubulin antibody as a loading control (bottom panel). Quantification of the specific bands from Western blots was performed using ImageJ software, and CHOP levels were normalized to tubulin levels. Histogram of five independent experiments shows a statistically significant increase in CHOP levels in patient fibroblasts compared to controls. The data were assessed with a one-way analysis of variance (ANOVA) followed by Tukey's multiple comparison test (** $P \leq 0.01$, *** $P \leq 0.001$).

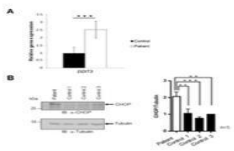

Figure 5
Fgure 5
27x17mm (300 x 300 DPI)

Figure 6: MEHMO Syndrome Belongs to the Disorders Associated with Alterations in eIF2 Function and Regulation or Involved in the UPR

To initiate translation the factor eIF2, a heterotrimeric complex of α, β and γ subunits, binds GTP and initiator Met-tRNA$_i^{Met}$ to form a ternary complex (TC). The TC associates with a ribosome, and during the course of translation initiation the GTP is hydrolyzed to GDP enabling release of eIF2–GDP from the ribosome. In order for eIF2 to participate in subsequent rounds of initiation, the GDP bound to eIF2 is exchanged for GTP in a reaction catalyzed by the guanine nucleotide exchange factor eIF2B. During ER stress, the recognition and refolding of misfolded proteins is assisted by the chaperones DNAJ3C and BiP with the help of the nucleotide exchange factor SIL1. The products of the *IER3IP1* and *WFS1* genes are also important for ER function. Under non-stress conditions BiP binds to the kinase PERK blocking its activation. The overload of misfolded proteins under stress conditions titrates BiP from PERK leading to activation of the kinase. Activated PERK phosphorylates the α subunit of eIF2, converting eIF2 into a competitive inhibitor of eIF2B. The subsequent decreased availability of eIF2–GTP for TC formation leads to downregulation of overall protein synthesis and increased translation of the *ATF4* mRNA. The ATF4 protein, a transcription factor, upregulates genes necessary for the adaptive response to the stress situation including *DDIT3* encoding CHOP. Prolonged activation of the stress response and elevated CHOP levels eventually leads to apoptosis. Mutations in genes involved in these processes (gray boxes: gene in red, disorder in black) account for syndromes with overlapping clinical pictures (summarized in Table 3).

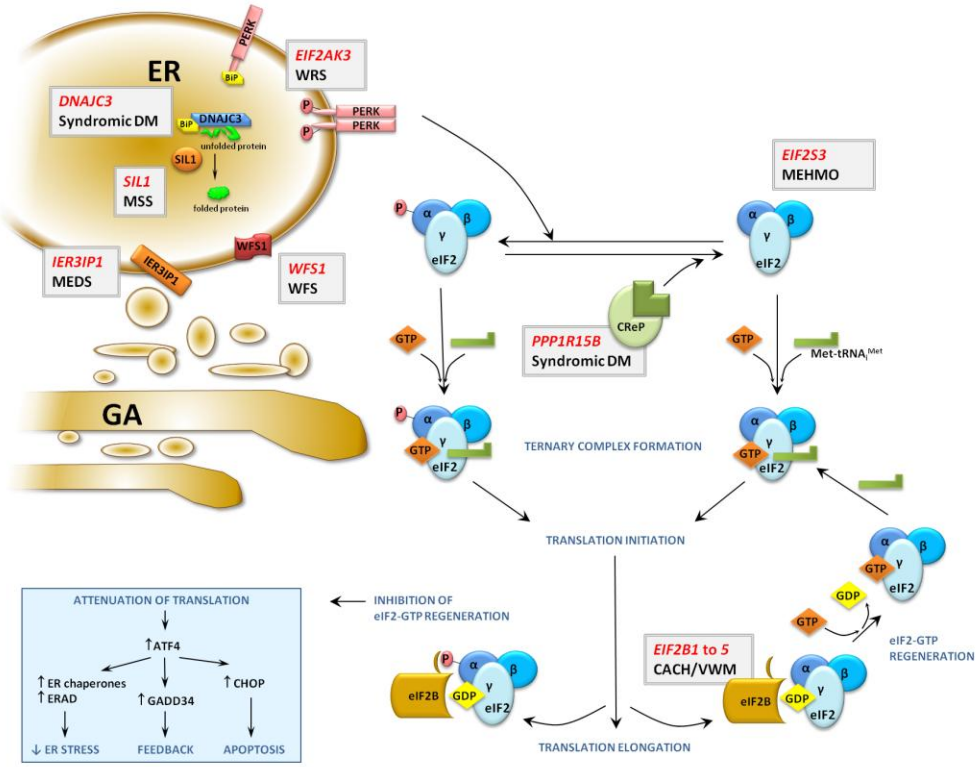

Table 1: Summary of phenotypes and genotypes of all cases with resolved and unresolved MEHMO syndrome.

Reference	**This study**	**This study**	**This study** (Steinmuller, et al., 1998)	**This study**	(Borck, et al., 2012)	(Moortgat, et al., 2016)	
Family	F1	F2	F3	F4	F5	F6	F7
***EIF2S3* genotype (NM_001415.3)**	c.1394_1397del TCAA (p.Ile465Serfs*4)	c.1394_1397del TCAA (p.Ile465Serfs*4)	c.1394_1397del TCAA (p.Ile465Serfs*4)	c.324T>A (p.Ser108Arg) VOUS	c.665T>C (p.Ile222Thr)	c.777T>G (p.Ile259Met)	c.1394_139 elTCAA(p.I 465Serfs*4
Origin	Slovakia	Slovakia	Germany	USA	Morocco Jewish	Belgium	Spain
# of described patients	1	1	4* (+1)	1	3	2	4
Lifespan	Alive at 5 y	Alive at 1,5 y	2 y / 7 / 2 / 10 mo	Alive at 5 y	Alive at 14 and 11,5 y	17y / Alive at 18 y	12 mo
Low birth weight	+	+	+ (1/4)	n.a.	n.a.	+	+
Low birth length	+	+	+ (1/2)	n.a.	n.a.	+	+
Full MEHMO syndrome (all clinical aspects of the acronym present)	+	+	+	-	-	-	+
Microcephaly	+	+	+	+	+	+	+
Seizures/abnormal EEG	+ (seizures + abnormal EEG)	+ (seizures without EEG correlate)	+	-	+ (1/3)	+ (1/2)	+

Brain MRI changes	+	+	n.a.	n.a.	+	+	+
Hypotonia	+ (axial)	+ (axial)	n.a.	+ (axial)	n.a.	+	-
Hypertonia	+ (peripheral)	+ (peripheral)	+	+ (spasticity)	+ (lower limb spasticity)	+ (for limbs spasticity)	+
Hyperreflexia	-	-	n.a.	-	+	n.a.	n.a.
Hypogonadism/genitalism	+	+	+	+, hypospadia	+ (post pubertal, 1/3)	+	+
Developmental delay	+	+	+	+	+	+	+
Infancy-onset obesity	+	+	+	+	+ (post pubertal, 1/3)	-	n.a.
Postnatal growth retardation	+	+	+	-	+	+	+
Hypoglycemia	Neonatal	Neonatal	n.a.	n.a.	n.a.	Episodic	Neonatal
Diabetes	Onset at 10 months	Onset at 10 months	Onset at age of 6 months (1/4)	-	-	-	-
Other Endocrinopathy	Panhypopituitarism	Partial hypopituitarism	Small thyroid (1/4)	-	Low GH levels (2/3)	-	-
Other	atrial septal defect, lactose intolerance, elevated hepatic enzymes, severe combined dyslipidaemia	-	Increased levels of acylcarnithine and fatty acids, single palmar crease (left hand), facial telangiectasia (1/5)	Chronic lung disease, congenital scoliosis, dysphagia, delayed gastric emptying, grade 5 vesico-ureteral reflux	Ataxic gait, Achilles tendon shortening, III:1 -cleft lip and palate, walked independently at 2 y, speaks short sentences, can feed himself; III:2 - speaks 3-4 words, cannot feed himself	Skeletal immaturity	-

cDNA nucleotide numbering uses +1 as the A of the ATG translation initiation codon in the reference sequence NM_001415.3, with the initiation codon as codon 1, VOUS – variant of unknown clinical significance, GH - growth hormone, n.a. - not available; * patient IV:8 was diagnosed prenatally with microcephaly and the pregnancy was terminated at week 24. MEGDEL: 3-Methylglutaconic Aciduria Type IV With Sensorineural Deafness, Encephalopathy and Leigh-Like Syndrome

Table 2: Respiratory chain complex II and IV activity measurements in permeabilized muscle fibers of index patient from family 1.

	Controls mean±SD	**Patient mean±SD**	**p**
Complex II	3.11±0.4	1.22±0.15	**0.009**
Complex IV	1.66±0.75	2.1±0.84	0.409

Activities are expressed in nM/min of consumed oxygen per mg of tissue wet weight.

Table 3: Similarities among syndromes caused by mutations in genes involved in eIF2 function or regulation or in the UPR.

Gene	EIF2S3	EIF2B1, 2, 3, 4, 5	PPP1R15B	EIF2AK3	IER3IP1	WFS1	DNAJC3	SIL1
protein	γ subunit of eIF2	Subunits of eIF2B	CReP (p-eIF2α phosphatase)	PERK (eIF2α kinase)	ER and Golgi located	ER transmembrane protein	BiP co-chaperone	BiP co-chaperone
Role in protein metabolism	Translation initiation	eIF2-GTP recycling for translation initiation	Constitutively restores translation initiation	UPR - downregulation of translation in case of ER stress	Modulation of apoptosis and differentiation	Ca^{2+} homeostasis important for correct protein folding	Ensures proper folding of proteins	Ensures proper folding of proteins
Inactivating mutations lead to	Attenuation of translation, inappropriate ATF4-CHOP induction	Attenuation of translation, inappropriate ATF4-CHOP induction	Attenuation of translation	Impaired ER stress induced attenuation of translation, lack of ATF4-CHOP branch of UPR induction, ER overload	Increased susceptibility to cellular stress	ER Ca^{2+} depletion and misfolding of proteins	Increased ER stress	Increased ER stress
Syndrome*	MEHMO (MIM# 300148), syndromic XLID	CACH/VWM (MIM# 603896)	Syndromic ID with diabetes (MIM# 616817)	WRS (MIM# 226980)	MEDS (MIM# 614231)	WFS (MIM# 222300)	ACPHD (MIM# 616192)	MSS (MIM# 248800)
Inheritance	X-linked recessive	AR	AR	AR	AR	AR	AR	AR
No. of patients/families (including this study)	18/8	~290	4/2	~60	7/5	>450	5/2	~70
Onset	Congenital	From congenital to adult	Congenital	Neonatal, first year of life	Congenital	Childhood	From child to adult	Congenital to infancy
Life span	Few months, oldest	Stress-induced death,	Oldest patient alive at 31 y	Few weeks to few years,	The oldest patient deceased at	30-40 years	Oldest patient alive at 41 y	

	patient alive at 18 y	childhood form - months to years from onset; adult form - years from onset		exceptionally over 30 y	8 y			
Diabetes	+/-	-	+	+	+	+	+	-
Obesity	+	-	-	-	+	-	-	-
Endocrinopathies	Panhypopituitarism, hypogenitalism, hypogonadism, +/-	-	Hypothyroidism +/-	Central hypothyroidism	Hypogenitalism, hypogonadism, +/-	Diabetes insipidus	n.r.	Hypergonadotrophic hypogonadism, +/-
ID	Moderate to profound	None to profound	Severe	None to severe	Profound	+/-	-, isolated cognitive deficit	Mild to moderate
Microcephaly	+	+/-	+	-	+	-	n.r.	+/-
Neurodegeneration	+	+	+	n.r.	+	+	+	+
Developmental delay	+	+ After disease onset	+	+	+	+/-	-	+
Epilepsy	+	+	n.r.	n.r.	+	-	-	+/-
Short stature	+	-	+	+	+/-	-	+	+
Bone abnormalities	+/-	-	+	Multiple epiphyseal dysplasia	+/-	-	n.r.	+
Hearing loss	-	-	-	-	-	+	+	-
Dysmorphic features	+	-	+	+/-	+		+	+/-
Special features		Ovarian failure, optic nerve		Liver dysfunction, recurrent		Optic atrophy, diabetes		Congenital cataracts, myopathy

		atrophy		infections		insipidus		
Progresive course	+	+	+	+	+	+	+	+
Episodic aggravation due to stress/illness	+	+	n.r.	+	+	-	n.r.	n.r.
References	This study; Borck et al., 2012; Moortgat et al., 2016; Steinmuller et al., 1998; Tarpey et al., 2009	Fogli, et al., 2004; Labauge et al., 2009	Abdel-Salam et al., 2012; Kernohan et al., 2015	Delepine, et al., 2000; Julier and Nicolino, 2010; Rubio-Cabezas, et al., 2009	Abdel-Salam et al., 2012; Poulton et al., 2011; Shalev, et al., 2014	de Heredia, et al., 2013; Fonseca et al., 2005	Synofzik et al., 2014	Ezgu, et al. 2014; Hasegawa, et al., 2014 Senderek e al., 2005

*CACH/VWM – childhood ataxia with central hypomyelination/vanishing white matter disease; WRS – Wolcott-Rallison syndrome; MEDS – microcephaly, epilepsy, and diabetes syndrome; WFS – Wolfram syndrome; ACPHD – ataxia, combined cerebellar and peripheral, with learning loss and diabetes mellitus; MSS – Marinesco-Sjörgen syndrome; BiP – immunoglobulin heavy-chain binding protein
Abbreviations: AR – autosomal recessive; n.r. – not reported

Reference	**This study**	**This study**	**This study** (Steinmuller, et al., 1998)	**This study**	(Borck, et al., 2012)	(Moortgat, et al., 2016)	
Family	F1	F2	F3	F4	F5	F6	F7
***EIF2S3* genotype (NM_001415.3)**	c.1394_1397delTCAA (p.Ile465Serfs*4)	c.1394_1397delTCAA (p.Ile465Serfs*4)	c.1394_1397delTCAA (p.Ile465Serfs*4)	c.324T>A (p.Ser108Arg) VOUS	c.665T>C (p.Ile222Thr)	c.777T>G (p.Ile259Met)	c.1394_139 elTCAA(p.I 465Serfs*4
Origin	Slovakia	Slovakia	Germany	USA	Morocco Jewish	Belgium	Spain
# of described patients	1	1	4* (+1)	1	3	2	4
Lifespan	Alive at 5 y	Alive at 1,5 y	2 y / 7 / 2 / 10 mo	Alive at 5 y	Alive at 14 and 11,5 y	17y / Alive at 18 y	12 mo
Low birth weight	+	+	+ (1/4)	n.a.	n.a.	+	+
Low birth length	+	+	+ (1/2)	n.a.	n.a.	+	+
Full MEHMO syndrome (all clinical aspects of the acronym present)	+	+	+	-	-	-	+
Microcephaly	+	+	+	+	+	+	+
Seizures/abnormal EEG	+ (seizures + abnormal EEG)	+ (seizures without EEG correlate)	+	-	+ (1/3)	+ (1/2)	+
Brain MRI changes	+	+	n.a.	n.a.	+	+	+
Hypotonia	+ (axial)	+ (axial)	n.a.	+ (axial)	n.a.	+	-
Hypertonia	+ (peripheral)	+ (peripheral)	+	+ (spasticity)	+ (lower limb spasticity)	+ (for limbs spasticity)	+

Hyperreflexia	-	-	n.a.	-	+	n.a.	n.a.
Hypogonadism/genitalism	+	+	+	+, hypospadia	+ (post pubertal, 1/3)	+	+
Developmental delay	+	+	+	+	+	+	+
Infancy-onset obesity	+	+	+	+	+ (post pubertal, 1/3)	-	n.a.
Postnatal growth retardation	+	+	+	-	+	+	+
Hypoglycemia	Neonatal	Neonatal	n.a.	n.a.	n.a.	Episodic	Neonatal
Diabetes	Onset at 10 months	Onset at 10 months	Onset at age of 6 months (1/4)	-	-	-	-
Other Endocrinopathy	Panhypopituitarism	Partial hypopituitarism	Small thyroid (1/4)	-	Low GH levels (2/3)	-	-
Other	atrial septal defect, lactose intolerance, elevated hepatic enzymes, severe combined dyslipidaemia	-	Increased levels of acylcarnithine and fatty acids, single palmar crease (left hand), facial telangiectasia (1/5)	Chronic lung disease, congenital scoliosis, dysphagia, delayed gastric emptying, grade 5 vesico-ureteral reflux	Ataxic gait, Achilles tendon shortening, III:1 -cleft lip and palate, walked independently at 2 y, speaks short sentences, can feed himself; III:2 - speaks 3-4 words, cannot feed himself	Skeletal immaturity	-

	Controls mean±SD	**Patient mean±SD**	**p**
Complex II	3.11±0.4	1.22±0.15	**0.009**
Complex IV	1.66±0.75	2.1±0.84	0.409

Activities are expressed in nM/min of consumed oxygen per mg of tissue wet weight.

Gene	***EIF2S3***	***EIF2B1, 2, 3, 4, 5***	***PPP1R15B***	***EIF2AK3***	***IER3IP1***
protein	γsubunit of eIF2	Subunits of eIF2B	CReP (p-eIF2α phosphatase)	PERK (eIF2αkinase)	ER and Golgi located
Role in protein metabolism	Translation initiation	eIF2-GTP recycling for translation initiation	Constitutively restores translation initiation	UPR - downregulation of translation in case of ER stress	Modulation of apoptosis and differentiation
Inactivating mutations lead to	Attenuation of translation, inappropriate ATF4-CHOP induction	Attenuation of translation, inappropriate ATF4-CHOP induction	Attenuation of translation	Impaired ER stress induced attenuation of translation, lack of ATF4-CHOP branch of UPR induction, ER overload	Increased susceptibility to cellular stress
Syndrome*	MEHMO (MIM# 300148), syndromic XLID	CACH/VWM (MIM# 603896)	Syndromic ID with diabetes (MIM# 616817)	WRS (MIM# 226980)	MEDS (MIM# 614231
Inheritance	X-linked recessive	AR	AR	AR	AR
No. of patients/ families (including this study)	18/8	~290	4/2	~60	7/5
Onset	Congenital	From congenital to adult	Congenital	Neonatal, first year of life	Congenital
Life span	Few months, oldest patient alive at 18 y	Stress-induced death, childhood form - months to years from onset; adult form - years from onset	Oldest patient alive at 31 y	Few weeks to few years, exceptionally over 30 y	The oldest patient deceased at 8 y
Diabetes	+/-	-	+	+	+
Obesity	+	-	-	-	+
Endocrinopathies	Panhypopituitarism, hypogenitalism, hypogonadism, +/-	-	Hypothyroidism +/-	Central hypothyroidism	Hypogenitalism, hypogonadism, +/-
ID	Moderate to profound	None to profound	Severe	None to severe	Profound

Microcephaly	+	+/-	+	-	+
Neurodegeneration	+	+	+	n.r.	+
Developmental delay	+	+ After disease onset	+	+	+
Epilepsy	+	+	n.r.	n.r.	+
Short stature	+	-	+	+	+/-
Bone abnormalities	+/-	-	+	Multiple epiphyseal dysplasia	+/-
Hearing loss	-	-	-	-	-
Dysmorphic features	+	-	+	+/-	+
Special features		Ovarian failure, optic nerve atrophy		Liver dysfunction, recurrent infections	
Progresive course	+	+	+	+	+
Episodic aggravation due to stress/illness	+	+	n.r.	+	+
References	This study; Borck, et al., 2012; Moortgat, et al., 2016; Steinmuller, et al., 1998; Tarpey, et al., 2009	Fogli, et al., 2004; Labauge, et al., 2009	Abdel-Salam, et al., 2012; Kernohan, et al., 2015	Delepine, et al., 2000; Julier, et al., 2010; Rubio-Cabezas, et al., 2009	Abdel-Salam, et al., 2012; Poulton, et al., 2011; Shalev, et al., 2014